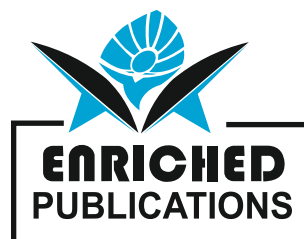


# **Journal of Mechanics and Thermodynamics**

**Volume No. 11  
Issue No. 2  
May - August 2023**



**ENRICHED PUBLICATIONS PVT. LTD**

**S-9, IInd FLOOR, MLU POCKET,  
MANISH ABHINAV PLAZA-II, ABOVE FEDERAL BANK,  
PLOT NO-5, SECTOR-5, DWARKA, NEW DELHI, INDIA-110075,  
PHONE: - + (91)-(11)-47026006**

# **Journal of Mechanics and Thermodynamics**

## **Aims and Scope**

Journal of Mechanics and Thermodynamics publishes theoretical and practice oriented papers, dealing with problems of modern technology (power and process engineering, structural and machine design, production engineering mechanism and materials, etc.), Materials and Design Engineering, Vibration and Control, Thermal Engineering and Fluids Engineering.

# **Journal of Mechanics and Thermodynamics**

**Managing Editor  
Mr. Amit Prasad**

**Editor in Chief**

**Dr. Syed Fahad Anwer**  
IIT, Kanpur  
sfahadanwer@zhcet.ac.in

# Journal of Mechanics and Thermodynamics

(Volume No. 11, Issue No. 2, May - August 2023)

## Contents

Sr. No	Article/ Authors	Pg No
01	The Effect of Heat Treatment on the Mechanical Behavior of FE- CR- AL based OPH Alloy <i>- Omid Khalaj, Hana Jirková, Adam Stehlik, Julie Volkmanová, Jiří Svoboda</i>	70 - 79
02	Photoluminescence Study of Carriers Confinement and Thermal Stability of INAS/INP (001) Quantum Dots Emitting Near 1.3 $\mu$ <i>- Fatiha Bsahraoui, Michel Gendry, Faouzi Saidi</i>	80 - 85
03	Development of High- Temperature Heat Exchangers using Advanced Manufacturing Technologies <i>- Martina Koukolikova, Pavel Podany</i>	86 - 93
04	Application of Selective Heating in Al-Steel Dissimilar Joining <i>- Pankaj Kaushik, Dheerendra Kumar Dwivedi</i>	94 - 101
05	Geometro Thermodynamics of the Boltzmann-GIBBS and Pareto Distributions <i>- Maria N. Quevedo</i>	102 - 108

---

# The Effect of Heat Treatment on the Mechanical Behavior of Fe- Cr- Al based OPH Alloy

<sup>1</sup> Omid Khalaj, <sup>2</sup> Hana Jirková, <sup>3</sup> Adam Stehlík, <sup>4</sup> Julie Volkmanová, <sup>5</sup> Jiří Svoboda

<sup>1,2,3,4</sup> Regional Technological Institute, University of West Bohemia, Univerzitní 22, 301 00, Pilsen, Czech Republic

<sup>5</sup> Institute of Physics of Materials, Academy of Sciences of The Czech Republic, Žižkova 22, 616 62, Brno, Czech Republic

E-mail: <sup>1</sup>khalaj@rti.zcu.cz, <sup>2</sup>hstankov@rti.zcu.cz, <sup>3</sup>stehlika@rti.zcu.cz, <sup>4</sup>volkmann@rti.zcu.cz, <sup>5</sup>svobj@ipm.cz

## **ABSTRACT**

*The Fe-Al Oxide Precipitation Hardened (OPH) alloy is new generation of Oxide Dispersion Strengthened (ODS) alloys which is famous group of material based on their high temperature properties. The general production process of OPH alloys consists of a mechanical alloying process to create a material with a ductile matrix and hard oxide dispersion. Two variants of Fe-Cr-Al based OPH alloys developed by the authors to investigate the thermomechanical properties under different conditions. The results show that the heat treatment has a significant role on the mechanical properties of OPH alloys as well as microstructure development. It can improve the ultimate tensile strength (UTS) up to 100% while improving the elongation to almost 20%.*

**Keywords - OPH Alloys, Fe-Al, Heat Treatment, ODS Alloys**

## **I. INTRODUCTION**

Iron Aluminum based OPH alloys are so nowadays interested because of low-cost and improved mechanical properties. By additional Cr contents of around 15 wt.%, it could be one of the leading candidates for structural components of future power plants [1-3]. Several advantages are considered when employing ferretic Fe-Cr-Al alloys in high temperature applications. In addition of lower raw material and preparation costs and of course superior oxidation resistance, the alloys have a higher melting point, lower density and lower thermal expansion compare to the current nickel or cobalt base alloys [4, 5]. Besides the oxidation resistance of Fe-Cr-Al ODS alloys is attributed to the presence of the yttrium as a reactive element and in fact this element leads to the formation of an adherent and slow growing Al<sub>2</sub>O<sub>3</sub> film exhibiting highly protective properties for the underlying material up to 1200°C [6]. However, the mechanical strength of these alloys in the cast and wrought condition at elevated temperatures were too low to make them outstanding for such a purpose, that's why the dispersion strengthening with stable oxide particle used to improve their higher temperature strength without sacrificing the excellent surface stability of the matrix alloy [7, 8]. ODS steels usually have reasonable creep resistance rather than their non-reinforced counterparts, however it usually suffer from poor toughness[9-11]. Therefore it is very important to optimize the microstructure of ODS steels to achieve an improved thermomechanical behavior. The author's previous experience showed that the use of

Y<sub>2</sub>O<sub>3</sub> is effective to adjust the oxygen content in Fe-Cr-Al OPH Alloys [12, 13]. In addition, this could also enhance the impact properties of OPH ferritic steels [14]. However, there exists little information about the annealing effect on the microstructure and tensile properties of these materials at elevated temperatures. Thus the authors tried to manufacture two variants of Fe-Cr-Al OPH alloys differing in milling time to investigate the effect of annealing on the thermomechanical properties of this group of alloys

## II. EXPERIMENTAL PROCEDURE

The OPH alloy was prepared based on Fe-Cr-Al matrix under a controlled mechanical alloying (MA) process. A particular advantage of the process is that the stored energy introduced to powders by high energy milling, can contribute to the production of a large elongated grain structure during subsequent high temperature heat treatments. However, special care should be considered for the milling time and rotation speed. The components consist of (wt.%) 71Fe-15Cr-6Al-3Mo-1Ta-4Y<sub>2</sub>O<sub>3</sub> in a form of atomized powder which then mixed with the specific amount of O<sub>2</sub> in form of gas in a low energy ball mill. The mill which is developed by the authors is capable of evacuation and filling by oxygen in addition of adjusting rotation speed. The milling lasted for 150 h for first variant (V1) and 230 h for the second variant (V2), both at 70 rpm. Then the powder became a solid solution and transferred to the rolling container in a vacuum condition. At the same time, it has been evacuated by suction pump and then sealed by means of welding. The final semi products went through two step hot rolling at 900°C and the final thickness of 6 mm covered by 1 mm steel container was achieved. Based on the type of tests, the desired sample shape then cut by means of waterjet, parallel to the rolling direction.

In order to investigate the effect of annealing on the thermomechanical properties of OPH alloys more in details, both variants were put under heat treatment described on table 1. Both variants then went through the tensile and hardness tests at room temperature (RT) to see how they were effected from the different heat treatment. A metallographic analysis was alsomade to go more in depth through the microstructure of these alloys.

Variant	Temperature (oC)	Holding time (hours)
V1	1000	5, 10
	1100	5, 10
	1200	1, 5, 10
V2	1000	5, 10
	1100	5, 10
	1200	1, 5, 10

**Table 1: Annealing plan**

---

### III. RESULTS AND DISCUSSIONS

The mechanical properties after heat treatment of both materials were investigated by performing the tensile test using a thermomechanical simulator which could keep the constant desire strain rate of 0.003 s<sup>-1</sup> during the whole test. Fig. 1 to Fig. 3 show the flow curves for both V<sub>1</sub> and V<sub>2</sub> under different annealing conditions which described in Table 1. It should be noted that all the tensile tests were done at RT. It can be seen that both UTS and elongation are significantly sensitive to heat treatment. In case of UTS, the best result achieved for V<sub>1</sub> after 20 hours of annealing at 1000 °C while the best elongation achieved for the same variant at 1200 °C after same holding time.

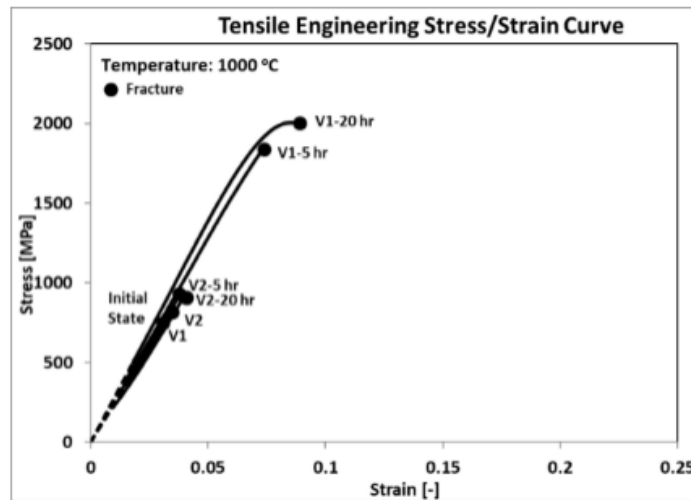


Figure 1: Flow curves after annealing at 1000 °C

On the other hand, annealing at higher temperature, increased the ductility of OPH alloy while at lower temperature, higher strength could be achieved, regardless of milling time. Compare to initial state (IS), the improvement in UTS could be varied from 20% after annealing at 1200 °C (Fig. 3) to more than 100% after annealing at 1000 °C (Fig. 1). The most effective one for V<sub>1</sub>, happened at 1100 °C holding for 20 hours, which increase the UTS for almost 50% while the elongation increased to 10%.

Besides, the results confirmed that higher milling time, caused less improvement on the mechanical properties of OPH Alloy, even after annealing at elevated temperatures. The UTS improvement for V<sub>2</sub> (higher milling time) after 20 hours annealing at 1000 °C and 1100 °C is almost 15% to 29%, respectively compare to initial state while no improvement in elongation was observed. It seems that the improvement for V<sub>2</sub> started at 1100 °C after 20 hours of annealing (Fig. 2) which then increased by increasing the annealing temperature to 1200 °C (Fig. 3). UTS increased almost by 30% and 43% after 5 and 20 hours respectively, compare to initial state.

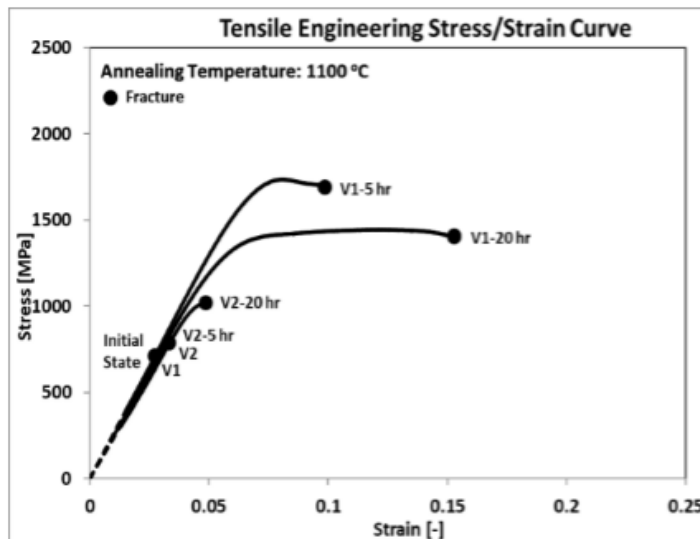


Figure 2: Flow curves after annealing at 1100 °C

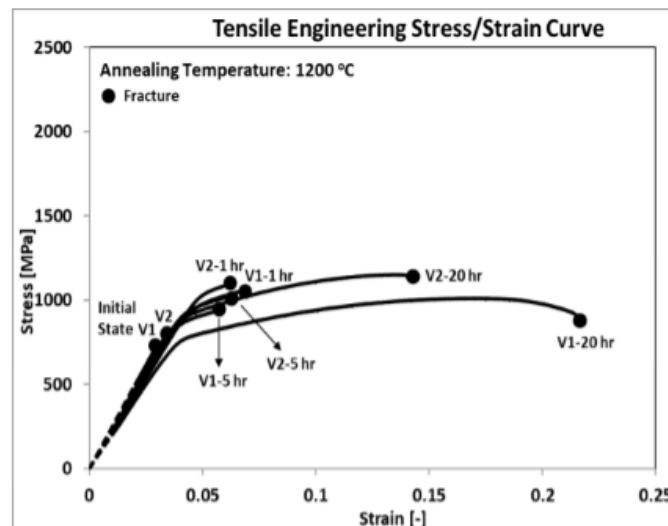
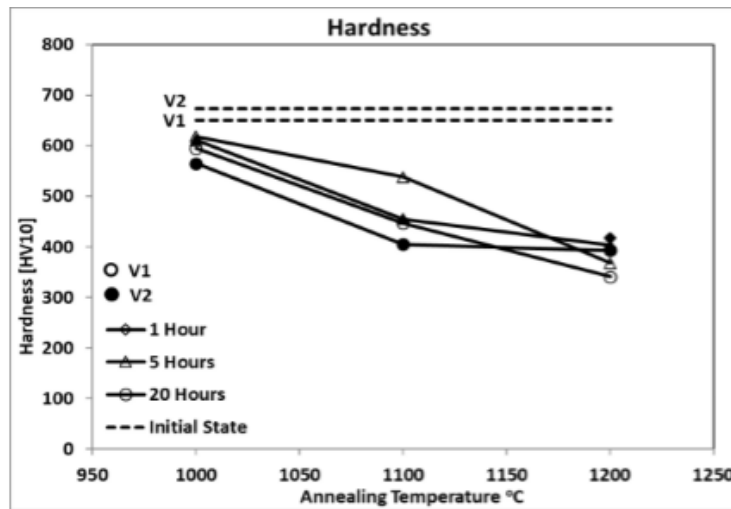


Figure 3: Flow curves after annealing at 1200 °C

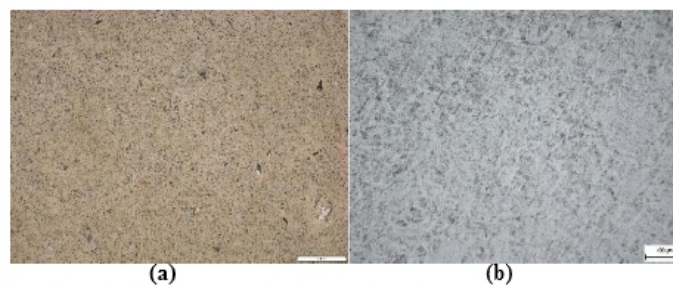
Figure 4 shows the hardness (HV10) results for both materials on the initial state and on the samples after annealing under heat treatment at 1000 C, 1100 C and 1200°C holding within the time described in table 1. The hardness test according to Vickers was performed by using a ZWICK/ROELL Z2.5 hardness tester with a load of 10 kg and loading time 11 s on the surface fracture area of polished samples. The average value was calculated from three measurements. The hardness of samples demonstrates the ability of OPH alloys to resist plastic deformation at various elevated temperatures. As the ODS ferritic steels possess remarkable mechanical properties such as high tensile and creep strength, OPH steels surely possess extremely hard surface and strength. Thus, Vickers hardness test is the standard method to measure the hardness of this group of materials compared to other hardness measurement methods such as Rockwell and Brinell.



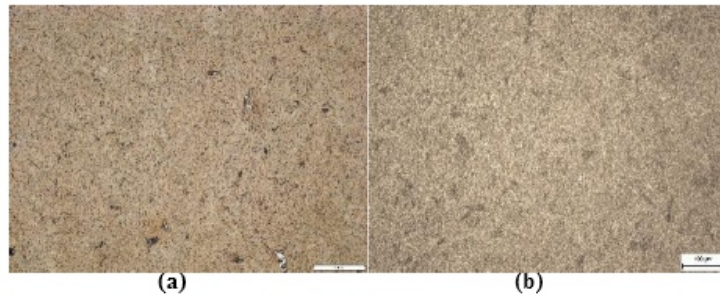
**Figure 4: Hardness (HV10) at different conditions**

The results show that the annealing also effected the hardness on both variants of OPH alloys. Compare to initial state, elevating temperature up to 1200°C decreases the hardness almost 30% while at 1000°C it decreases maximum 10%. Besides,  $V_1$  after 5 hours annealing at 1100°C shows less reduction in HV10 compare to the  $V_2$  at the same condition. The reason could be attributed to the recrystallization process which may not started in this situation for  $V_1$  [15]. On the other hand, the decrease in HV10 is more considerable at the first step of annealing from 1000°C to 1100°C, however on the second step from 1100°C to 1200°C, less reduction happened. On the other hand, longer holding time has more influence on the hardness value of OPH alloys. Holding for 20 hours up to 1100°C decreases the hardness 2 times more compare to similar condition with less holding time while at 1200°C, longer holding time has the same influence as lower time.

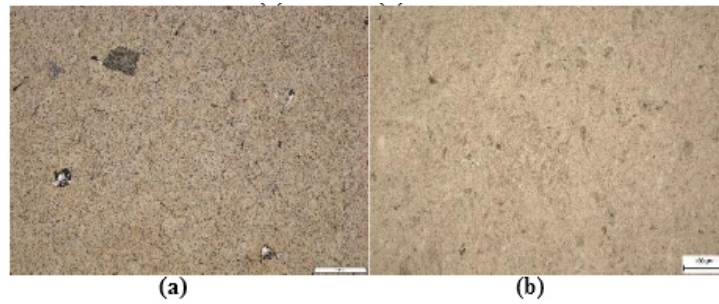
In order to go more in depth, the microstructure of both OPH variants with different annealing conditions were investigated. Fig. 5 to 11 show the microstructure of all both  $V_1$  and  $V_2$  material using optical microscope. It could be seen that after the rolling (initial state), the microstructure of both materials consisted of solid solution with very fine oxides with different chemical composition. The microstructure was homogeneous without visible cracks after rolling. This microstructure keeps its formation with almost no changes in the main structure up to annealing at 1100°C for 5 hours, especially for  $V_2$  (Fig. 7b). However, recrystallization did not take place in the entire material volume. Very small grains were still visible in the microstructure.



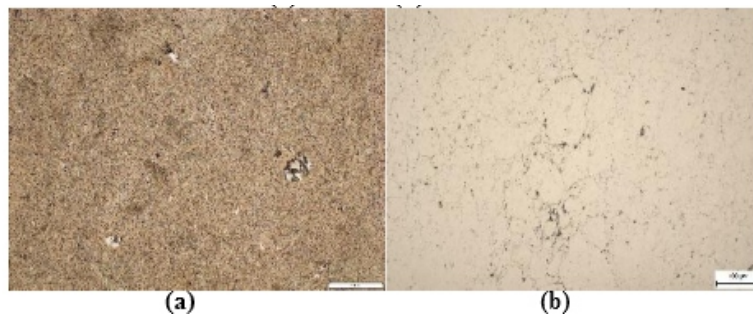
**Figure 5: OPH alloys microstructure (Initial State), (a) $V_1$  and (b)  $V_2$**



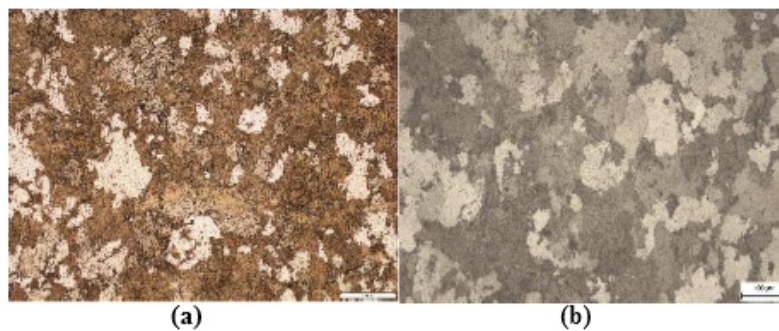
**Figure 6: OPH alloys microstructure (1000°C, 5 hours), (a)  $V_1$  and (b)  $V_2$**



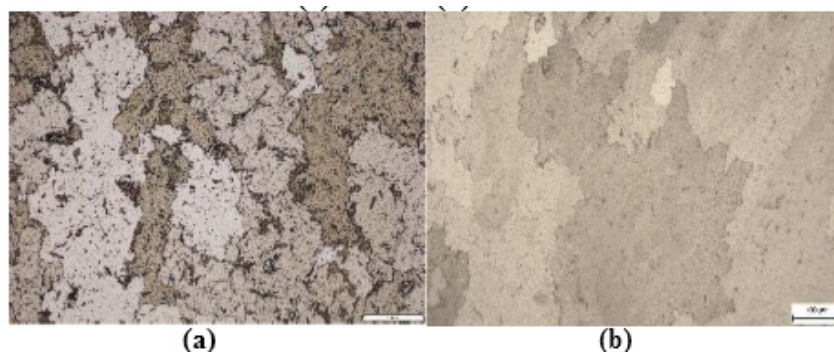
**Figure 6: OPH alloys microstructure (1000°C, 20 hours), (a)  $V^1$  and (b)  $V^2$**



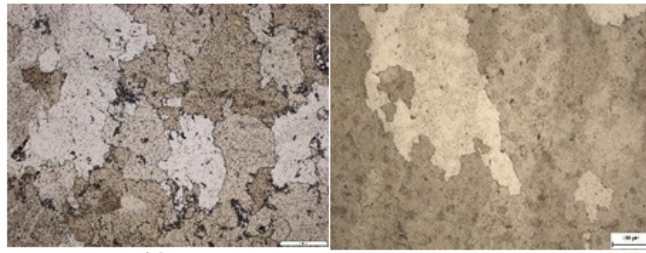
**Figure 7: OPH alloys microstructure (1100°C, 5 hours), (a)  $V_1$  and (b)  $V_2$**



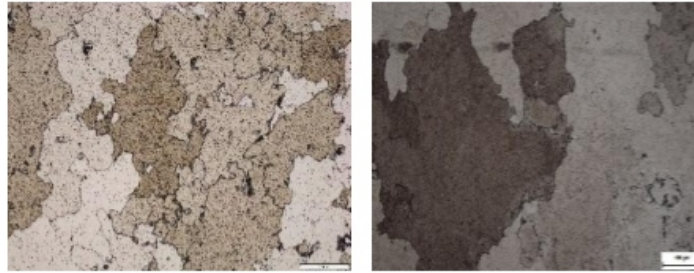
**Figure 8: OPH alloys microstructure (1100°C, 20 hours), (a)  $V_1$  and (b)  $V_2$**



**Figure 9: OPH alloys microstructure (1200°C, 1 hour), (a)  $V_1$  and (b)  $V_2$**



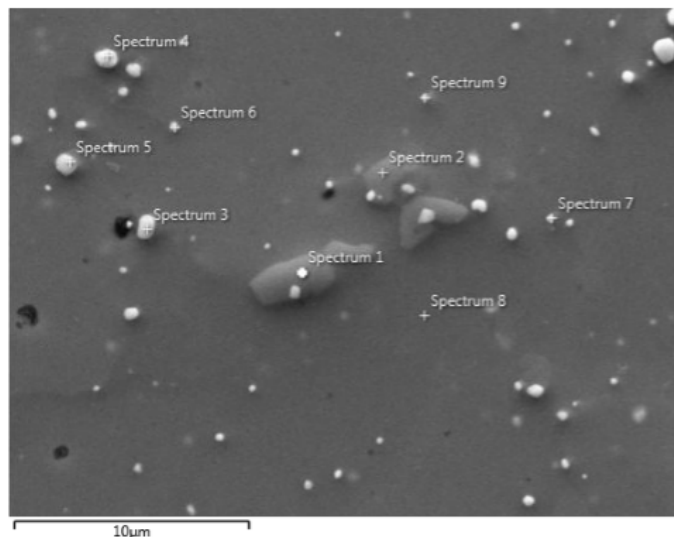
**Figure 10: OPH alloys microstructure (1200°C, 5 hours), (a) V<sub>1</sub> and (b) V<sub>2</sub>**



**Figure 11: OPH alloys microstructure (1200°C, 20 hours), (a) V<sub>1</sub> and (b) V<sub>2</sub>**

Following Fig. 8, the recrystallization also starts for V<sub>1</sub> holding at 1100°C for 20 hours (Fig. 8a) while it was started at the same temperature for 5 hours for V<sub>2</sub> (Fig. 7b). The recrystallization progress almost completed for both variants after 1 hours at 1200°C (Fig. 9) and followed by Fig. 11 that shows the longest holding time of 20 hours at 1200°C, which the structure was completely recrystallized. The results also showed that the grain size is bigger for the V<sub>2</sub> materials with longer milling time.

To have a better understanding of chemical composition of the occurring particles in the microstructure of initial state, an EDS spectrum analysis were performed on both variants using scanning electron microscope (Zeiss Crossbeam 340- 47-44) (Fig. 12, Fig. 13) In the material V<sub>1</sub> two types of particles were found. The bigger particles were darker and the EDS analysis showed that they are molybdenum, chromium, aluminum rich (Fig. 12). The second type were smaller lighter particles, which also contained tantalum.



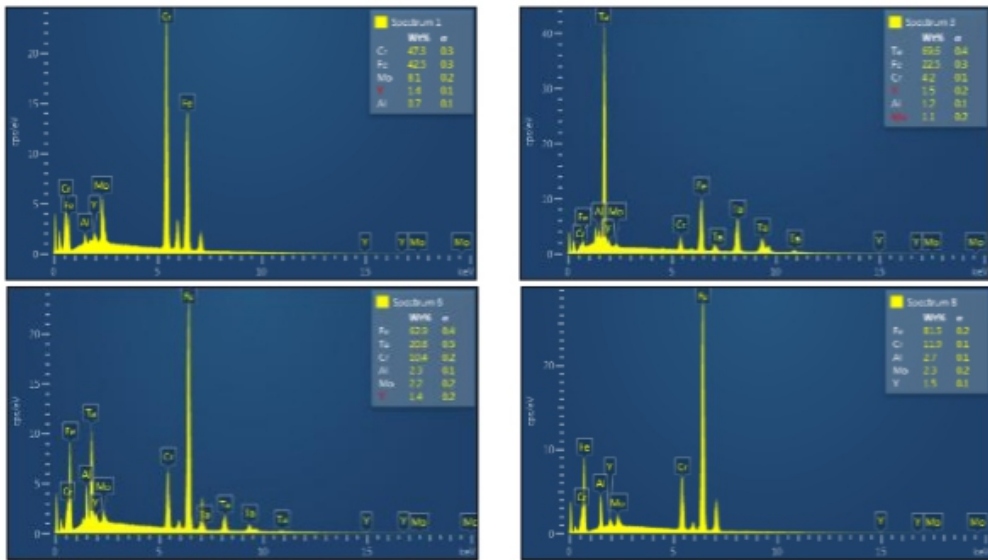
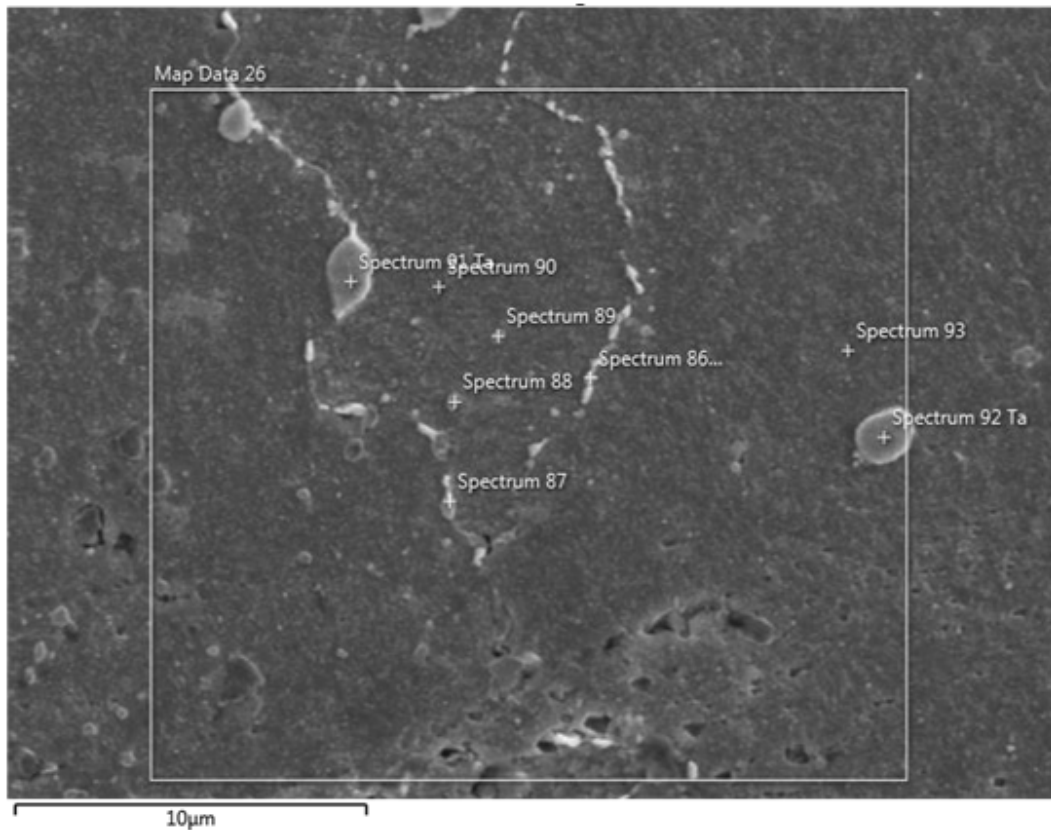
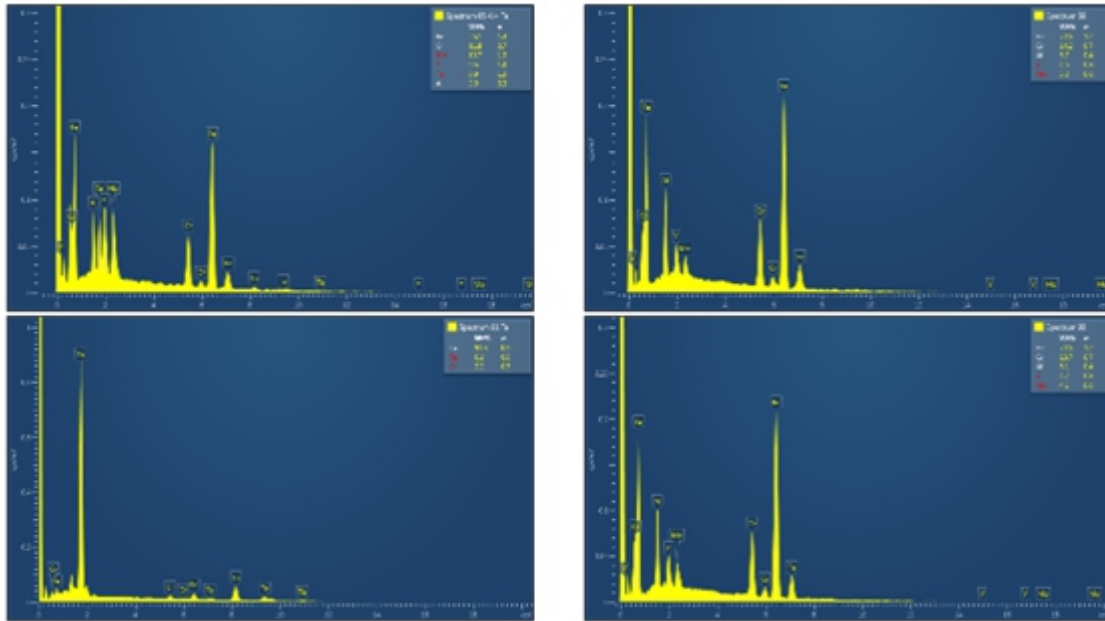


Figure 12: EDS spectrum analysis results for  $V_1$

On the other hand, the bigger particles in  $V_2$  (Fig. 13) were tantalum rich and the rest of the particles were Fe-Cr-Al rich. Molybdenum and chromium as a refractory element increases significantly the cohesive strength of the grain boundaries, stabilize bcc-lattice and increase the oxidation resistance at high temperatures. However, both elements increase the stability of carbides precipitating at grain boundaries provoking intergranular fracture.





**Figure 13: EDS spectrum analysis results for  $V_2$**

#### IV. CONCLUSION

This paper described a preliminary investigation on the effect of annealing on the thermomechanical properties, hardness and microstructural of two variants of OPH alloys, differing in milling time, using a number of different tests. The results show that the heat treatment at elevated temperatures has a significant role on the mechanical properties as well as microstructure development of these alloys. The optimum annealing condition could be reported as  $1100^{\circ}\text{C}$  for 20 hours which has the optimum effect on both UTS and elongation. Besides, it was found out that longer milling time ( $V_2$ ) has a negative influence on the mechanical properties which caused the late starting of recrystallization process. Base on that, the  $V_2$  showed less sensitive to heat treatment even at higher temperature with longer holding time. On the other hand, the hardness value ( $Hv_{10}$ ), shows a decrease to almost 50% of initial value while the heat treatment temperature increased from  $1000^{\circ}\text{C}$  to  $1200^{\circ}\text{C}$ . Also higher reduction was observed from the second step of temperature increasing ( $1100^{\circ}\text{C}$  to  $1200^{\circ}\text{C}$ ) compare to the first step ( $1000^{\circ}\text{C}$  to  $1100^{\circ}\text{C}$ ). The microstructure observation showed that the recrystallization, which leads to grain growth, started after holding for 5 hours ( $V_1$ ) and 20 hours ( $V_2$ ) at  $1100^{\circ}\text{C}$ . Before this critical temperature, the structure was composed from very fine grains of about 100 nm. Over critical annealing temperature, a full recrystallized structure with coarse grains was obtained. Besides, the EDS analysis confirmed the presence of chromium and molybdenum in the biggest particles and tantalum was found in the smaller, which showed a positive behavior within the microstructures of OPH alloys.

---

## ACKNOWLEDGMENT

This paper includes results created within the project 17-01641S Improvement of Properties and Complex Characterization of New Generation Fe-Al-O Based Oxide Precipitation Hardened Steels subsidized by the Czech Science Foundation from specific resources of the state budget of the Czech Republic for research and development.

## REFERENCES

- [1] O. Khalaj, H. Jirková, T. Janda, L. Kucerova, and J. Svoboda, "Improving the High Temperature Properties of a New Generation of Fe-Al-O Oxide Precipitation Hardened Steels," *Materials and technology*, vol. 53, no. 4, pp. 495-504, 2019.
- [2] R. L. J. J. o. N. M. Klueh, "Reduced-activation steels: Future development for improved creep strength," vol. 378, no. 2, pp. 159-166, 2008.
- [3] J. Svoboda et al., "Microstructure Evolution in ODS Alloys with a High-Volume Fraction of Nano Oxides," vol. 8, no. 12, p. 1079, 2018.
- [4] O. Khalaj, H. Jirková, B. Masek, P. Hassasroudsari, T. Studecky, and J. Svoboda, "Using thermomechanical treatments to improve the grain growth of new-generation ODS alloys," *Materials and technology*, vol. 52, no. 4, pp. 475-482, 2018.
- [5] S. Ohtsuka, S. Ukai, M. Fujiwara, T. Kaito, T. J. J. o. p. Narita, and c. o. solids, "Nano-structure control in ODS martensitic steels by means of selecting titanium and oxygen contents," vol. 66, no. 2-4, pp. 571-575, 2005.
- [6] G. Merceron, R. Molins, and J. L. Strudel, "Oxidation behaviour and microstructural evolution of FeCrAl ODS alloys at high temperature," *Materials at High Temperatures*, vol. 17, no. 1, pp. 149-157, 2000/01/01 2000.
- [7] B. Masek, O. Khalaj, H. Jirkova, J. Svoboda, and D. J. M. I. T. Bublikova, "Influence of thermomechanical treatment on the grain-growth behaviour of new Fe-Al based alloys with fine Al<sub>2</sub>O<sub>3</sub> precipitates," vol. 51, no. 5, pp. 759-768, 2017.
- [8] K. Murty and I. J. J. o. N. M. Charit, "Structural materials for Gen-IV nuclear reactors: Challenges and opportunities," vol. 383, no. 1-2, pp. 189-195, 2008.
- [9] O. Khalaj, B. Masek, H. Jirkova, A. Ronesova, and J. Svoboda, "Investigation on New Creep and Oxidation Resistant Materials," *Materials and technology*, vol. 49, no. 4, pp. 645-651, 2015.
- [10] G. Odette, M. Alinger, and B. J. A. R. M. R. Wirth, "Recent developments in irradiation-resistant steels," vol. 38, pp. 471- 503, 2008.
- [11] J. Svoboda and P. J. A. M. Lukáš, "Creep deformation modelling of superalloy single crystals," vol. 48, no. 10, pp. 2519-2528, 2000.
- [12] O. Khalaj, H. Jirková, B. Mašek, and J. Svoboda, "Microstructure Evaluation of New ODS Alloys with Fe-Al Matrix and Al<sub>2</sub>O<sub>3</sub> Particles," in *Proceedings of the 2017 International Conference on Industrial Design Engineering*, 2017, pp. 11-15: ACM.
- [13] H. J. Xu, Z. Lu, D. M. Wang, Z. W. Zhang, Y. F. Han, and C. M. Liu, "Structure and composition of oxides in FeCrAl ODS alloy with Zr addition," (in English), *Materials Science and Technology*, vol. 33, no. 15, pp. 1790-1795, 2017.
- [14] Z. Oksiuta, M. Lewandowska, P. Unifantowicz, N. Baluc, K. J. F. E. Kurzydowski, and Design, "Influence of Y<sub>2</sub>O<sub>3</sub> and Fe<sub>2</sub>Y additions on the formation of nano-scale oxide particles and the mechanical properties of an ODS RAF steel," vol. 86, no. 9-11, pp. 2417-2420, 2011.
- [15] F. M. Shamsudin, S. Radiman, Y. Abdullah, and N. A. J. S. M. Hamid, "The effect of annealing to the hardness of high Y<sub>2</sub>O<sub>3</sub>-oxide dispersion strengthened (ODS) ferritic steels," vol. 47, no. 1, pp. 189-193, 2018.

---

---

# Photoluminescence Study of Carriers Confinement and Thermal Stability of InAs/InP (001) Quantum Dots Emitting Near 1.3 $\mu\text{M}$

<sup>1</sup>Fatiha Bsahraoui, <sup>2</sup>Michel Gendry, <sup>3</sup>Faouzi Saidi

<sup>1,2,3</sup>Sciences and Technology Institute University center of Tissemsilt Algeria, Nanotechnologies Institute of Lyon (INL) University of Lyon France, Micro-Optoelectronic and Nanostructures Laboratory University of Monastir Tunisia  
E-mail: <sup>1</sup>fatiha.besahraoui@yahoo.fr

## **ABSTRACT**

*Photoluminescence Spectroscopy (PLS) measurements have been performed on self-organized InAs quantum dots (QDs) grown on InP(001) nominal substrate. The lowest full width at half maximum (FWHM) of the PL spectrum measured at low temperature and at high excitation power, indicates the good carrier confinement and low size dispersion of InAs/InP(001) QDs. Through the excitation power-PL measurements with the help of an explicit law, which express the variation of PL intensity with the excitation power, we have evidenced the presence of two families of InAs QDs which have a good carrier confinement and an emission wavelength around 1.3  $\mu\text{m}$ . This result gives the possibility to use this sample in optical telecommunications and in infrared photodetectors sensitive on broad spectral bands.*

**Keywords-** *Photoluminescence, Quantum dots, Self-organized Growth, Optical Telecommunication.*

## **I. INTRODUCTION**

In recent years, there was a great interest in self-organized quantum dots (QDs) structures [1]. This interest comes from the different applications of these nanostructures in performed optoelectronic devices such as lasers, infrared photodetectors, and optical telecommunication [2]. InAs QDs grown on InP substrate are actually considered as a good element used for the emission wavelength in 1.3-1.55  $\mu\text{m}$  range especially in optoelectronic devices used for long haul telecommunications [3]. In this paper, we study the carrier confinement in InAs/InP(001) grow in Stranski-Krastanov (SK) mode using Solid Source Molecular Beam Epitaxy (MBE) method. This study has been carried out by using the Photoluminescence Spectroscopy (PLS) measurements. We identify the spatial confinement and the origin of different observed PL peaks through the evolution of PL spectra with the excitation density.

## **II. EXPERIMENTS**

The InAs/InP quantum dots investigated in this paper were grown by Solid Source Molecular Beam Epitaxy (MBE) in a Riber 2300 reactor. They were grown on semi-insulating InP(001) substrate. A buffer layer of InP with 200nm of thickness was grown at 480°C using a phosphorus pressure equals to  $1.10^{-5}$  Torr. Then three monolayers (ML) of InAs were grown at 520°C under an arsenic pressure fixed

at 2.10<sup>-6</sup> Torr. The elaborated sample is not intentionally n-type doped (about 10<sup>16</sup> cm<sup>-3</sup>). After that, the sample was capped with an InP capping layer of a 300-nm-thick. The PL spectra were obtained in the 0.4–400 mW excitation density range. The sample was excited using the 514.5 nm line of an Ar–Kr ion laser. The emitted light was dispersed by a spectrometer and detected by a thermoelectrically cooled InGaAs photodetector using a conventional lock-in technique.

### III. RESULTS AND DISCUSSIONS

#### A. Spatial Confinement

The photoluminescence intensity is related to the excitation power through the following explicit law [4]:

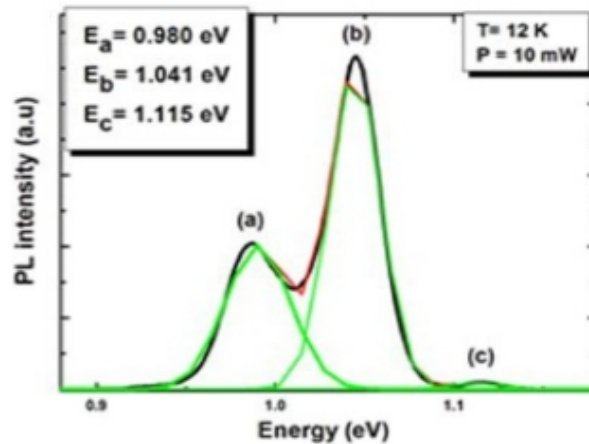
$$I = P_{ex}^n \quad (1)$$

$n \geq 1$  for excitonic recombinations.

$n = 1$  for intrinsic recombinations (band to band).

$n \leq 0.8 - 0.9$  for impurities recombinations.

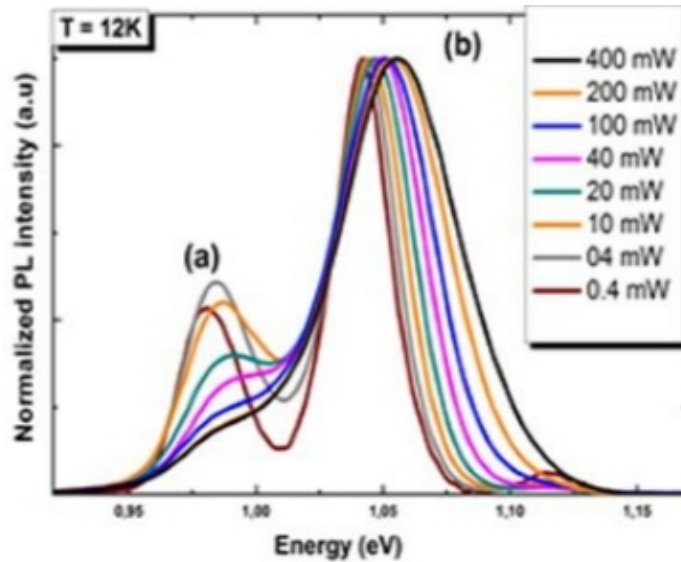
The Fig. 1 presents the PL spectrum of InAs/InP(001) QDs measured at 12 K and at low excitation power (10 mW).



**Fig. 1 PL spectrum at 12 K of InAs/InP(001) quantum dots.**

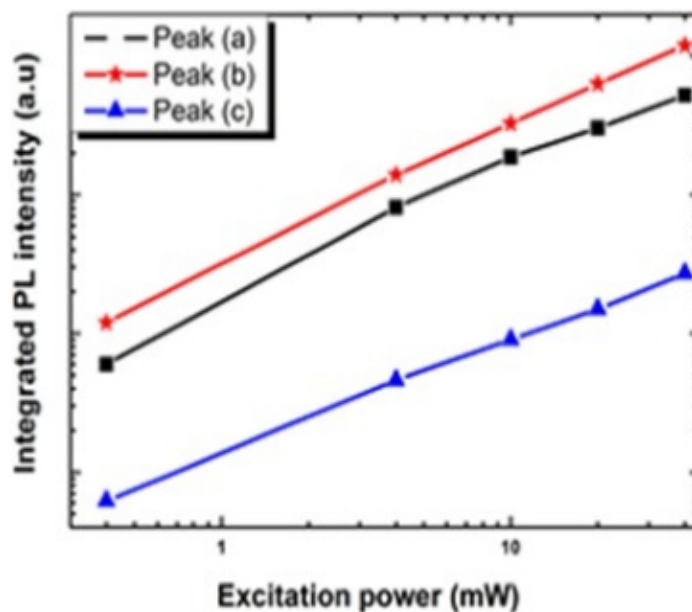
The spectrum shows a three emission bands. These emission bands can be adjusted to a three Gaussian peaks (a), (b) and (c) located in 0.980–1.115 eV energy range. The measured Full Width at Half Maximum (FWHM) is about 31 meV. This weak value of the FWHM indicates that these nanostructures of InAs/InP(001) have a good spatial confinement of photogenerated carriers compared to another InAs/GaAs(001) QDs[5]. In order to check the origin of the different observed PL peaks and the type of the corresponding transition (intrinsic, excitonic, defects, etc.). We propose a study of the luminescence as a function of excitation power. This study will be given by using the explicit law mentioned in (1).

Fig. 2 depicts the evolution of the normalized PL spectra of InAs/InP(001) QDs as a function of the excitation power. We note that there is no relative saturation of the PL peaks and no new peaks appeared when the excitation power increases [6]. This leads to suppose that the different observed peaks are attributed to ground states of families of QDs and/or to a defect states or traps related to the doped sample.



**Fig. 2 PL spectra at 12 K of InAs/InP(001) quantum dots measured at different excitation density of Ar-Kr ion laser.**

We have obtained the same behavior through the study of the integrated PL curves given as a function of excitation power as shown in Fig. 3.



**Fig. 3 Integrated PL spectra of InAs/InP(001) quantum dots as a function of excitation density.**

---

According to the explicit low given in (1), we deduce that the peaks (a) and (b) are attributed to intrinsic or band-to-band radiative transitions. On the other hand, the peak (c) is related to an extrinsic radiative transitions related to a defect states or traps related to the n type doping.

### A. Thermal Stability

Fig.4 presents the integrated PL intensity curve obtained in 12-300 K temperature range. The calculated ratio of the integrated PL intensity between 12 K and 300 K equals 9. This result provides the strong spatial quantum confinement of photogenerated carriers in this sample compared with other confined nanostructures [7]. Which leads to have a thermal stability. This property is very important to produce optoelectronic devices with a good optical quality such as lasers.

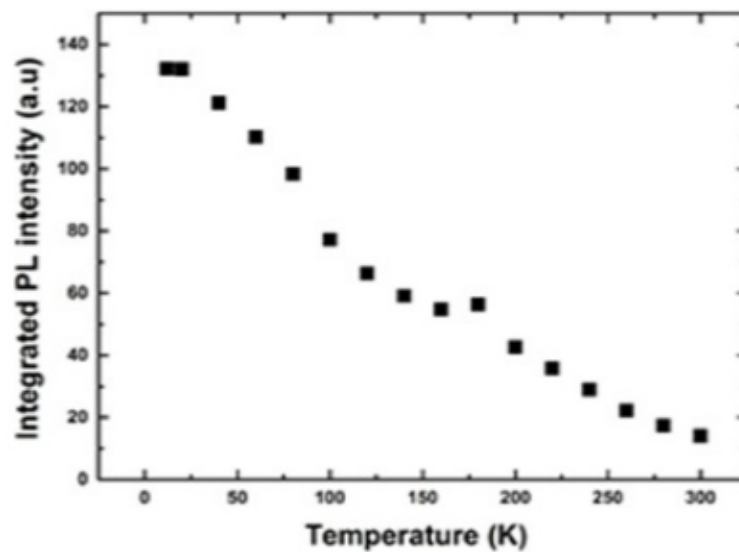


**Fig. 4 Integrated PL intensity of InAs/InP(001) QDs as a function of the temperature.**

## IV. CONCLUSION

Through the study of the PL spectra as a function of the excitation, we have deduced that our sample have not an excited energy levels. Note that, this behavior is traduced by the appearance of a new PL peaks when the excitation power increases. By introducing the explicit low of PL intensity, we have evidenced the presence of ground states of two families of InAs/InP(001) quantum dots of different size. The integrated PL spectra of InAs/InP(001) QDs have indicated the strong PL maintaining until room temperature of this sample. All these properties give the opportunity to use this sample in different optoelectronic devices such as microlasers emitting around 1.3  $\mu\text{m}$  with good optical gain, infrared photodetectors which have a good sensitivity on a wide energy range.

---

## REFERENCE

- [1] R. Seguin, A. Schliwa, S. Rodt, K. Pötschke, U. W. Pohl, and D. Bimberg, “Size-Dependent Fine-Structure Splitting in Self Organized InAs/GaAs Quantum Dots”, *Phys. Rev. Lett.*, vol. 95, pp. 257402, December 2005.
- [2] F. Klopf, R. Krebs, J.P. Reithmaier and A. Forchel, “High-temperature operating 1.3  $\mu\text{m}$  quantum-dot lasers for telecommunication applications”, *IEEE Photonics Technology Letters*, vol 13, pp. 764 - 766, August 2001.
- [3] H. Z. Song, T. Usuki, S. Hirose, K. Takemoto, Y. Nakata, and N. Yokoyama, “Site-controlled photoluminescence telecommunication wavelength from InAs/InP quantum dots”, *Appl. Phys. Lett.*, vol 86, pp. 113118, February 2005.
- [4] B. Salem, “Spectroscopie optique des îlots quantiques d’InAs/InP(001) pour la réalisation de composants optoélectroniques émettant à 1.55  $\mu\text{m}$ ”, Doctorat thesis, National Institute of applied Sciences of Lyon, France, 2003.
- [5] Denis Guimard, Ryo Morihara, Damien Bordel, Katsuaki Tanabe, Yuki Wakayama, Masao Nishioka, and Yasuhiko Arakawa, “Fabrication of InAs/GaAs quantum dot solar cells with enhanced photocurrent and without degradation of open circuit voltage”, *Appl. Phys. Lett.* vol 96, pp. 203507, May 2010.
- [6] M. Bayer, O. Stern, P. Hawrylak, S. Fafard, A. Forchel, “Hidden symmetries in the energy levels of excitonic ‘artificial atoms’”, *Nature.*, vol. 405, pp. 923-926, 2000.
- [7] Z. Y. Xu, Z. D. Lu, X. P. Yang, Z. L. Yuan, B. Z. Zheng, J. Z. Xu, “Carrier relaxation and thermal activation of localized excitons in self-organized InAs multilayers grown on GaAs substrates”, *Phys. Rev. B*, vol. 54, pp. 11528-11531, 1996.



---

# Development of High- Temperature Heat Exchangers using Advanced Manufacturing Technologies

<sup>1</sup> Martina Koukolikova, <sup>2</sup> Pavel Podany

<sup>1,2</sup>COMTES FHT A.S., Department of Materials Analysis, Prumyslova 995, 334 41 Dobrany, Czechia

E-mail: <sup>1</sup>mkoukolikova@comtesfht.cz, <sup>2</sup>ppodany@comtesfht.cz

## **ABSTRACT**

*Experimental program Development of high-temperature heat exchangers using advanced manufacturing technologies, mechanical design and materials was focused on the prototype production of the heat exchangers by means of conventional and progressive manufacturing methods. Developments in the additive manufacturing (AM) processes and the introduction of new and / or modified alloys gave engineers liberty not only in the design. Metallographic characteristics of the nickel-based alloys were the main objectives of the research. The results will contribute to the design and construction of the plate heat exchanger.*

**Keywords - Heat Exchangers, Superalloys, Additive Manufacturing.**

## **I. INTRODUCTION**

The main objectives of the project Development of high-temperature heat exchangers using advanced manufacturing technologies, mechanical design and materials is to design new types of the high-temperature gas/gas heat exchanger for applications in industrial and energy sectors, as well as for the new generation of nuclear reactors. The materials, which are applied in these sectors, are either stainless steels or nickel superalloys.

Nickel-based alloys have become standard for high-temperature applications. These alloys generally offer high corrosion and wear resistance when exposed to high temperatures. Conventional production of these alloys is well established; however boom in the field of additive manufacturing has opened a new way of the manufacturing procedure. The investigated components were processed from Incoloy alloy 800 HT (1.4959) and Inconel 718, materials ideal for high-temperature applications such as gas turbine parts, instrumentation parts, power and process industry parts up to 700 - 800 °C [1] - [3].

Materials produced by AM exhibit specificities compared to commonly produced components. From a material perspective, AM products show a strong dependence on the process parameters. The entire process chain of the additive manufacturing, which will be in near future similarly important to conventional methods, also highly influences the microstructure of the component. AM products are composed of tiny weld beads so-called “melt pools”, generated by the laser. A certain pattern of texture can be expected due to the fast and directional solidification. The resultant heat transfer and fluid flow

affect the size and shape of the melt pools, the cooling rate, and the transformation reactions in the melt pool and heat-affected zone[4] - [7]. Metallographic characteristics were performed by means of optical and scanning electron microscopy enhanced by electron backscattering diffraction analysis, a unique tool for assessing the material texture. After the literature search on the materials used nowadays for high-temperature heat exchangers, austenitic steels and nickel alloys were proposed for this research. This contribution will deal with the analysis of nickel alloys.

## II. EXPERIMENT DESCRIPTION

The experiment consisted of two main parts. In the first part, microstructural characteristics of the conventionally produced nickel-iron-chromium alloy Incoloy 800 HT (1.4959), was tested and analysed in as - received and aged conditions at 650 and 850 °C with 150 hours holding time. As not every material was found to be suitable for additive manufacturing, further tests were performed with the material Inconel 718. Direct Metal Laser Sintering (AM) method was involved in the second part of the experiment. The additively manufactured Inconel 718 was stress-relieved at 980 °C for 1 hour and air cooled.

The chemical composition of the alloys was measured by optical emission spectrometer BRUKER Q4 TASMAN. The results are given in Legend: LM (Light microscopy). Hardness HV 10 was measured according to ISO 6507 – 1 on Struers Durascan 50 (See Table II).

### Legend: LM (Light microscopy)

Alloy	Element (wt. %)							
	C	Si	Mn	Cr	Ni	Al	Ti	Fe
800 HT	0.07	0.26	0.8	19.93	31.1	0.46	0.57	bal.
IN 718	0.06	0.06	0.09	18.45	53.06	0.5	0.98	17.96

affect the size and shape of the melt pools, the cooling rate, and the transformation reactions in the melt pool and heat-affected zone[4] - [7]. Metallographic characteristics were performed by means of optical and scanning electron microscopy enhanced by electron backscattering diffraction analysis, a unique tool for assessing the material texture. After the literature search on the materials used nowadays for high-temperature heat exchangers, austenitic steels and nickel alloys were proposed for this research. This contribution will deal with the analysis of nickel alloys.

## II. EXPERIMENT DESCRIPTION

The experiment consisted of two main parts. In the first part, microstructural characteristics of the conventionally produced nickel-iron-chromium alloy Incoloy 800 HT (1.4959), was tested and analysed in as - received and aged conditions at 650 and 850 °C with 150 hours holding time. As not

---

every material was found to be suitable for additive manufacturing, further tests were performed with the material Inconel 718. Direct Metal Laser Sintering (AM) method was involved in the second part of the experiment. The additively manufactured Inconel 718 was stress-relieved at 980 °C for 1 hour and air cooled.

The chemical composition of the alloys was measured by optical emission spectrometer BRUKER Q4 TASMEN. The results are given in Legend: LM (Light microscopy). Hardness HV 10 was measured according to ISO 6507 – 1 on Struers Durascan 50 (See Table II).

**Legend: LM (Light microscopy)**



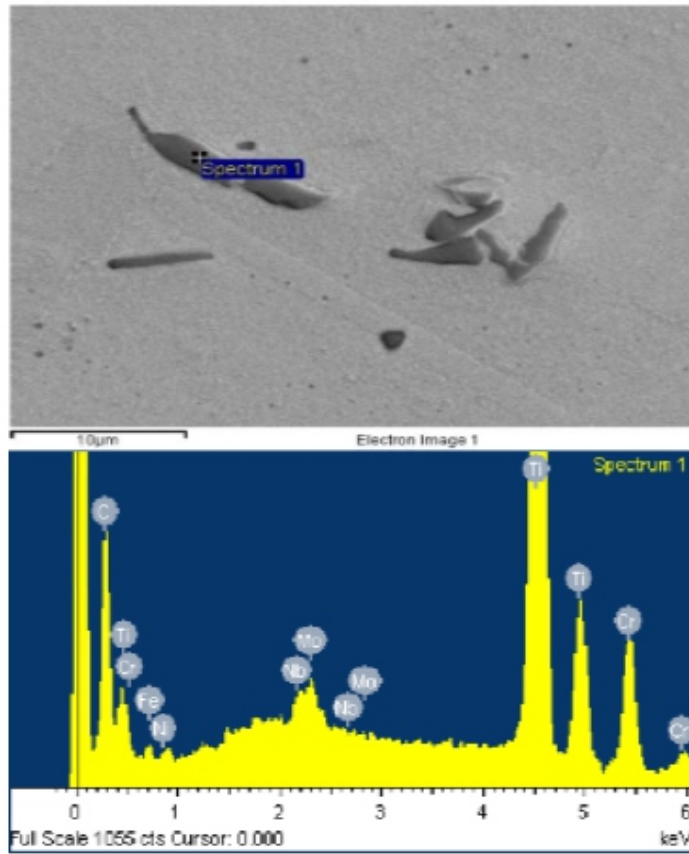
**Fig. 1 Incoloy 800 HT \_as\_ recieved state. LM**



**Fig. 2 Incoloy 800 HT 650°C - 150 h. LM**



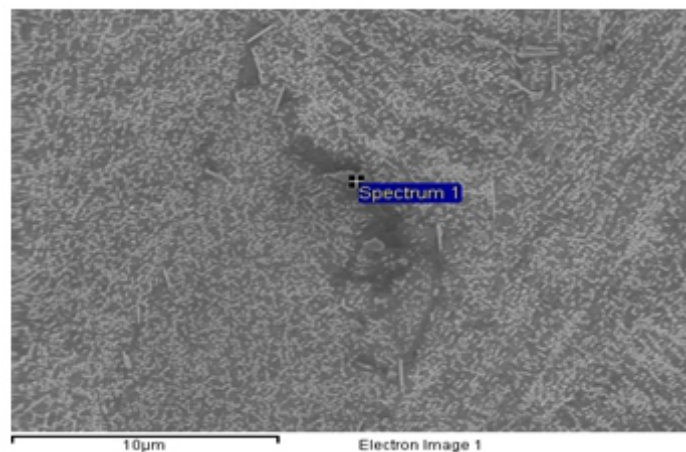
**Fig. 3 Incoloy 800 HT \_850°C - 150 h. LM**



**Fig. 4** Results of EDX measurements on Incoloy 800HT specimen on particles within the grains



**Fig. 5** IN 718\_LM



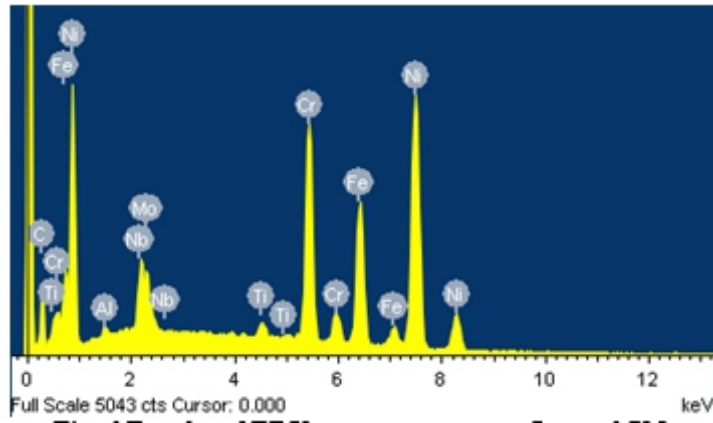


**Fig. 6 Results of EDX measurements on Inconel 718**

Specimen		HV10
Incoloy 800 HT	As received	120
	650°C - 150 h	183
	850°C – 150 h	142
Inconel 718	As received	387

**Table II. Results of hardness testing**

### B. Electron Backscatter Diffraction Analysis (EBSD)

The microstructure of Inconel 718 consists of an austenitic matrix with the presence of columnar grains in the Z-building direction. Fig. 7 shows band contrast - image quality. This indicates the "sharpness" of the Kikuchi lines for each index point. The lighter the point in the image (in the grayscale), the diffraction pattern of the Kikuchi line is sharper at that point. By default, the smallest sharpness (and hence the darker points in the picture) is achieved by indexing at grain boundaries, phase intervals, pores, inclusions, etc.

Fig. 8 shows the orientation of the individual grains of phases using the Inverse Pole Figure (an inverted pole pattern). In the Inverse Pole Figure are projected spheres aligned with the directions of the crystals. Sketched directions are a stereographic design of the directions of the crystals parallel to the normal direction(ND), the parallel direction (RD) or the transverse direction (TD) in the sample. An inverse pole pattern can help to visualize certain types of textures. Thus we can determine that, for example, the grain has the same orientation of the crystal lattice as several grains coloured with an identical colour. Fast and directional cooling during the AM processing resulted in a certain degree of texture, which is obvious from Fig. 9.

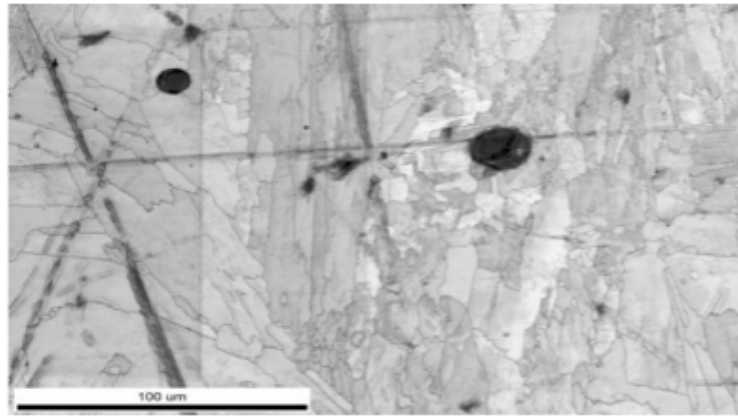


**Fig. 7 IQImage**

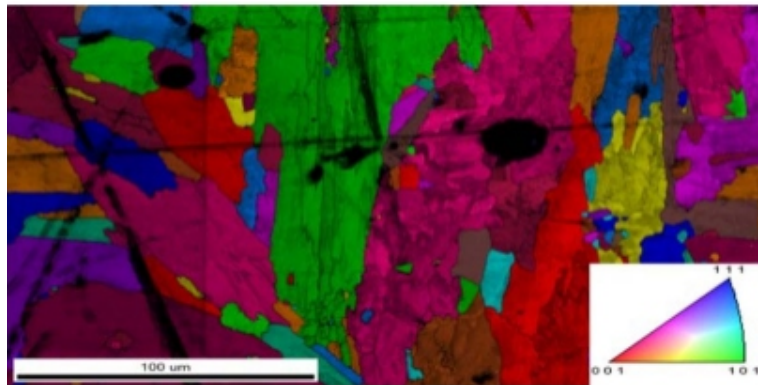


**Fig. 8 IPF - IQ Image**

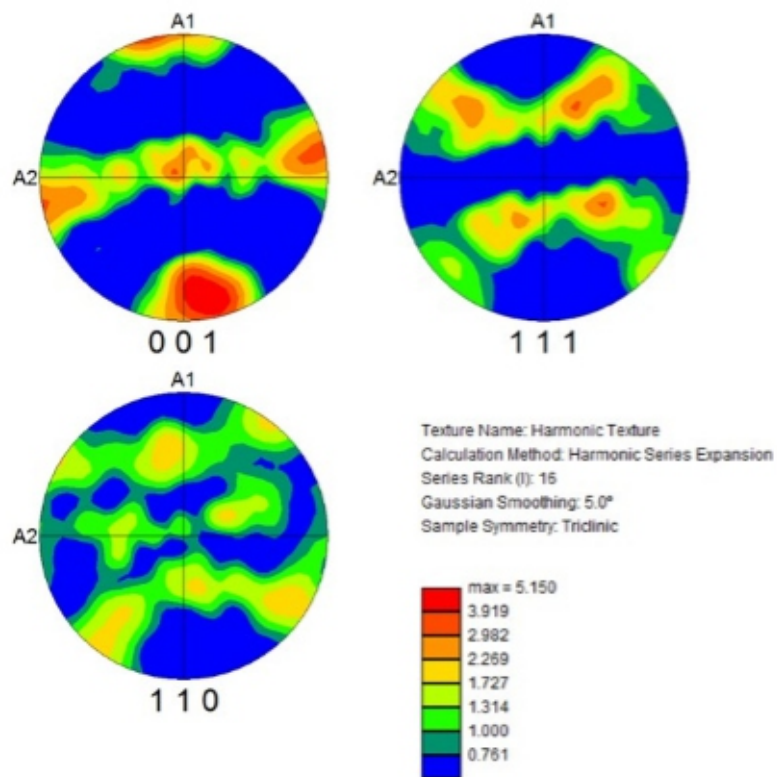


**Fig. 9 EBSD analysis pole figures**

---

### III. CONCLUSION

Two nickel alloys were selected for experiment dealing with micro structural properties of conventionally and additively manufactured superalloys. The grain size of conventionally manufactured Incoloy 800HT was not affected after ageing at two temperatures 650 and 850°C. Nevertheless, the precipitation of carbides within the grains and on the boundaries was observed in this material. The micro structure of additively manufactured material considerably differed from that of conventionally produced alloy, as fast and directional cooling took place during the processing. Presence of precipitates in the nickel-chromium alloy Inconel 718 micro structure, contributed to the strengthening of the matrix, which was reflected in the increase in hardness values. The DMLS processed heat exchanger will be tested in the experimental helium loop. The test results will serve mainly for the design and construction of a short-time service helium-helium heat exchanger.

### ACKNOWLEDGEMENT

The research paper was created within the project Development of high-temperature heat exchangers using advanced manufacturing technologies, mechanical design and materials. No.: FV10472, financed by the Ministry of Industry and Trade of the Czech Republic.

### REFERENCES

- [1] J. R. Davis, "Nickel, cobalt and their alloys", 2000.
- [2] Material data sheet. EOS Nickel Alloy IN718. TMS, WEIL/05.2014, EOS GmbH., 2014
- [3] ASM Handbook, Volume 9, Metallography and Microstructure, 2004.
- [4] D. I. Wimpenny; P. M. Pandey, and L. J. Kumar, "Advances in 3D Printing & Additive Manufacturing Technologies," ISBN 978-981-10-0812-2, pp. 40 - 53, 2017.
- [5] T.S. Srivatsan, T.S. Sudarshan, "Additive Manufacturing: Innovations, Advances, and Applications," ISBN 978-1-4987-1478-5, pp. 70 - 76, 2016.
- [6] M. Brandt, "Laser Additive Manufacturing: Materials, Design, Technologies, and Applications," pp. 55 - 70, ISBN 978-0-08-100434-0, 2017.
- [7] D. Gu, "Laser Additive Manufacturing of High-Performance Materials," ISBN 978-3-662-46089-4, pp. 223 - 271, 2015.



---

# Application of Selective Heating in Al-Steel Dissimilar Joining

<sup>1</sup>Pankaj Kaushik, <sup>2</sup> Dheerendra Kumar Dwivedi

<sup>1,2</sup>Department of Mechanical and Industrial Engineering, Indian Institute of Technology Roorkee, Uttarakhand, 247667, India

E-mail: <sup>1</sup>pkaushik4@me.iitr.ac.in, <sup>2</sup>dkd04fme@iitr.ac.in

## ABSTRACT

*Al-steel dissimilar joining has the advantages of both the materials in a single unit. This combination of materials has high industrial applicability. There is a large difference in physical, thermal and metallurgical properties of both the materials, which makes it difficult to join combination. In present work, the solid state joining of commercially pure aluminum and steel was performed. A number of attempts have been reported in the literature regarding preheating of steel to achieve better weld amalgamation. Earlier approaches were not much effective due to wide-spreading of heat in both plates. Thus, in this work, selective heating of steel side was performed using an induction heating equipment to avoid the heating of the aluminum side. Further, weld joints made by conventional friction stir welding (FSW) and newly developed induction heat-assisted FSW (IHAFSW) were compared using tensile testing and micrograph analysis. It was found that the elongation is improved up to 35% in hybrid welding which was a major concern in FSW. Detached debris of steel was alleviated and bonding surface area was increased in selective preheating which suggest higher ductility and in a sound weld joint.*

**Keywords—** Deformation, Friction stir welding(FSW), Hybrid joining, Induction heating, Intermetallic, solid welding, Unconventional.

## I. INTRODUCTION

Multi-material design of materials is a concept of combining two or more differently equipped material systems to take advantage of the properties of both. An example of such a combination can be Al-steel joint. Steel and aluminum are the most exploited materials in today's industrial world. They have affable availability in nature and perform suitably in almost every application. The area of application of both the metals is very vast. Their combination has also many applications in automobile, marine, shipbuilding, cryogenics and in aerospace industries. Steel has high strength and rigidity whereas aluminum has a high strength to weight ratio and good corrosion resistance. All of these properties are essential for the automotive industry. A combination of these two metals in a single unit provides good strength as well as weight saving, which in turn saves a lot of energy in the automotive industry. Honda in their fabrication of subframe (used in Honda accord) used Al-steel joint and compared its properties with conventionally formed frame and attained a 50% power saving as shown in Fig. 1.

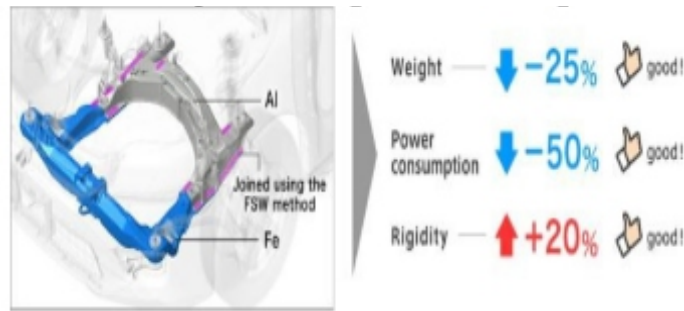


**Fig. 1 Frame fabricated by Honda using steel-aluminum joining [1]**

Regardless of its high applicability, this combination of metals is rarely used in industries due to various difficulties encountered during joining of these materials. The main issues related to the joining of steel with aluminum alloys are inferior strength and ductility of joint and a narrow process window. The predominant reason for lack of strength and ductility in case of fusion welding is insolubility of both the metal systems. There is an enormous difference in their physical and metallurgical properties. The properties associated mainly with welding of Al-steel are melting temperature, the coefficient of thermal expansion, thermal conductivity and strength. There is a huge difference in properties of these two material systems as shown in Table I. This difference in properties causes problems like non-uniform solidification, different thermal cycle, complex stresses, and differential expansion and contraction in case of fusion welding.

Non-fusion welding processes have an advantage over fusion welding processes in joining of Al-steel due to the elimination of fusion and solidification. The main concern in this metal combination is its insolubility in the molten state which is shunned in solid joining.

Properties	Steel	Aluminum
Melting temperature (°C)	1425-1540	463-671
Coefficient of thermal expansion ( $10^{-6} (\text{°C})^{-1}$ )	11.3-12.3	21.5-23.8
Conduction coefficient (W/m K)	45	235
Tensile strength (MPa)	247	90

**Table I Difference in physical properties of steel and aluminum [2]**

In solid-state joining techniques, various factors like heat generated by means of friction and plastic deformation, intermetallic compound formation and process parameters are to be critically balanced in order to get a sound joint. In friction stir joining of these metals, the most important property is the plastic behavior of the metals under high temperature. Thus, to bring both metals on the same level of strength and plasticity, the steel is heated and brought to a lower strength. Upon heating steel turns soft and its

plasticity comes in comparison to that of aluminum. Stirring becomes easier, and both materials mix up in a better way. Therefore, to bring down the steel to a lower strength, heat-assisted friction stir welding is examined by researchers. GTAW assisted hybrid FSW was used to join Al6061-T6 and STS304 stainless steel of 3 mm sheet by [3]. A sound joint was reported with the hybrid process and the strength of the joint was found to be higher than normal FSW joint. An electric current assisted friction stir welding setup was developed by [4] and joined steel and Al-Mg alloys. In his investigation, a variable current was applied and its effect on grain size was compiled. On increasing electric current in the circuit, the grain size in the weld zone was found to be increasing. A setup of electrically assisted friction stir welding was established by [5]. Al6061 alloy was welded with TRIP 780 steel. In his study, the tool of FSW was kept outside the circuit and various configurations of heating were tried. The combination of electro-plastic effect and joule effect aided in plunging and reduced the axial welding force. It was concluded that micro-interlocking can be seen in electric aided FSW at the Al-steel interface. This can inhibit the crack initiation and propagation of the intermetallic layer. In solid state joining of Al-steel, steel side is not actively taking part in joining. Thus to have an active stirring of steel plate without too much disintegration and fragment formation, selective preheating of steel plate is a viable approach. Therefore, researchers have shifted their attention towards hybrid processes in recent years.

## II. EXPERIMENTAL METHODOLOGY

Commercially pure aluminum and mild steel plates of dimension 150 mm × 50 mm and thickness 3 mm were placed in square butt configuration for pilot experiments. The tool made of tungsten carbide (WC) was used for FSW. The dimensions of the tool are specified in Table II.

After initial trials, the sound joint was obtained on welding process parameters of 708 RPM and weld scanning speed of 40 mm/min. For selective preheating trials, an induction heater (15KW) of the medium frequency range (30-100 KHz) is employed. A schematic of the system is shown in Fig. 2.

Tool shoulder diameter	Pin diameter	Pin length	Pin taper angle	Tool tilt angle
25 mm	6-8 mm	2.8 mm	20°	1°

**Table II Dimensions of tool used for welding**

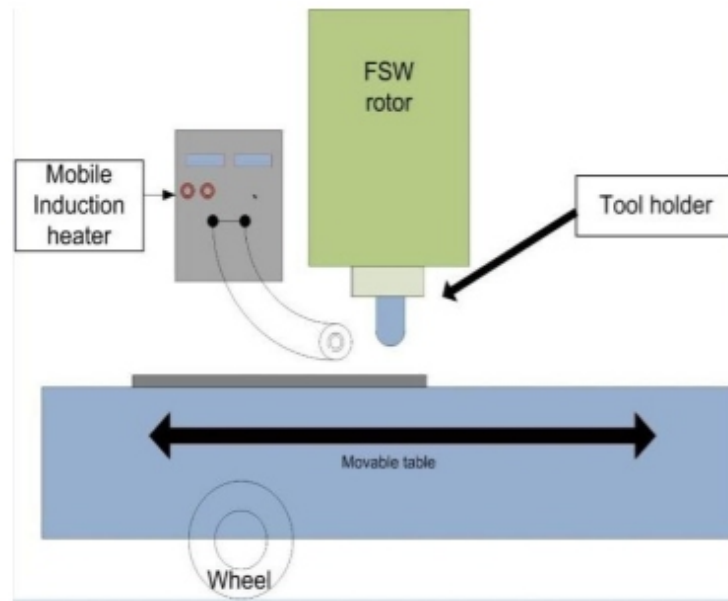


**Fig. 2 Schematic view of IHAFSW Setup**

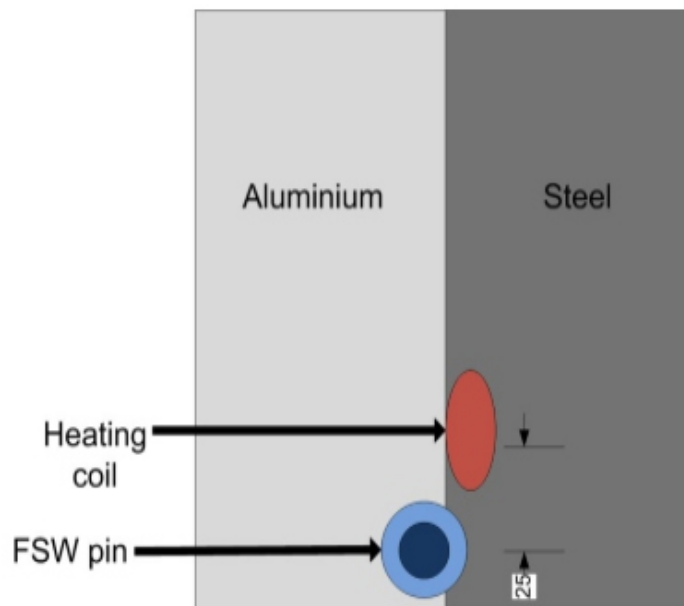


**Fig. 3 Location of FSW tool and Heating coil**

The coil of the Induction heater is placed over the steel plate at a distance of 25 mm ahead of the FSW tool as shown in Fig. 3. The distance between the coil and tool was kept constant during welding, The temperature was measured using k-type thermocouples placed in steel and aluminum plates during normal friction stir welding. The temperature of plates was measured by a Digital LCD IR pyrometer during induction heating process. The tensile specimen was prepared according to ASTM E8 standard. Tensile testing was performed on the universal tensile testing machine (Instron USA; model - 5980) at a cross-head speed of 1 mm/min. Samples were machined and polished using standard metallographic practices for microstructure study. Field emission scanning electron microscopy (FESEM) was used for microanalysis of the interface.

---

### III. RESULTS AND DISCUSSION

FSW is fundamentally a process of deformation on the application of a high strain rate. Additionally, thermal softening of the material takes place due to frictional heating. Material near around tool pin flows plastically. The flow stress of any material depends largely on its temperature. Thus, the temperature is a major factor in dissimilar friction stir welding.

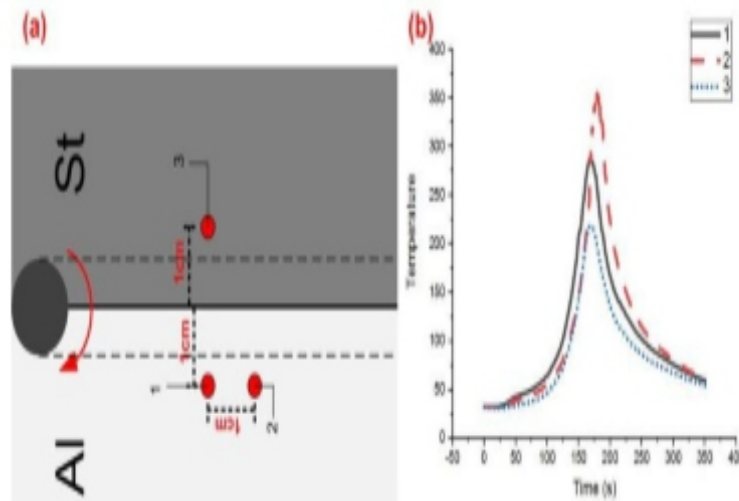


**Fig. 4 (a) Placement of thermocouples, and (b) Temperature vs time graph**

The temperature of the steel and aluminum plate was measured during welding using three k-type thermocouples. Thermocouples were placed in both the plates at a distance of 1 cm away from the centerline as shown in Fig. 4(a). Temperature vs time relationship during FSW is shown in Fig. 4(b). Peak temperature attained in steel plate during Friction stir welding was 219°C.

It has been shown in the weld thermal cycle that the peak was obtained at around 170 seconds after the starting of the tool rotation. The peak temperature achieved for the aluminum plate was 288°C at location 1 and 356°C for location 2. Thermocouple 2 was placed away from the initial weld start point. Thermocouple 1 and 3 attained peak temperature at the same time whereas 2 attains its peak temperature after 180 seconds. Heat is conducted in the whole Al plate very fast because of the high conductivity of aluminum. Therefore, thermocouple 2 showed the highest temperature because of the accumulation of heat of friction stirring and conduction.

The melting point of steel is around 1425°C - 1540°C. steel tends to get soften at a higher temperature and its strength becomes half of the original strength at 500°C [6]. Strength of steel decreases drastically and ductility is increased on the application of heat and the same is also confirmed by [7] as shown in Fig. 5. As discussed above, the temperature achieved during normal FSW was around 220°C for steel plate. This temperature is not sufficient for easy flowability of steel.

Thus to bring steel to an easily deformable state, we need to assist the FSW by some additional source of heating. There are a number of ways to preheat the steel sheet, for example:- TIG, Laser, Gas torch, induction heating, and electrical resistance heating. Selective heating of the plate can only be realized by induction heating. Therefore, to preheat the limited area of steel plate, Induction heating was selected.

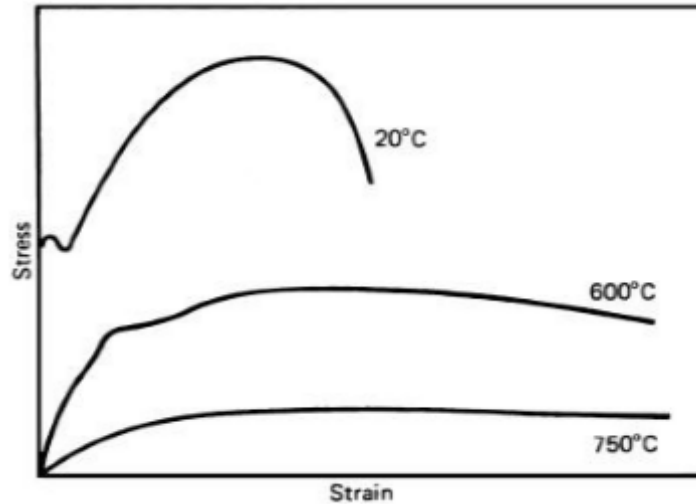


**Fig. 5 Stress-strain curve of mild steel at various temperatures [7]**

Induction heater works on the principle of eddy current and magnetic hysteresis loss, which only occurs in magnetic materials. Thus on induction heating, only steel plate gets heated and aluminum plate remains unaffected. Although some amount of heat was conducted towards the aluminum side, that was not sufficient to cause melting. Upon induction preheating, the temperature attained during welding was maintained around 600°C. Steel became soft and started flowing plastically during stirring action of FSW tool instead of breaking as a fragment. Macrographs of welds obtained from two different joining processes are shown in Fig. 6. In normal FSW joint, serrated steel fragments were observed. These fragments were detached from the parent steel plate and came in the aluminum matrix. In IHAFSW; the problem of detachment was avoided and extended finger like strand was present. Presence of an elongated fiber indicated the improvement of ductility of steel plate in IHAFSW. The bonding surface area was visibly increased in IHAFSW and it avoided the stress concentration and void formation associated with the detached fragment.

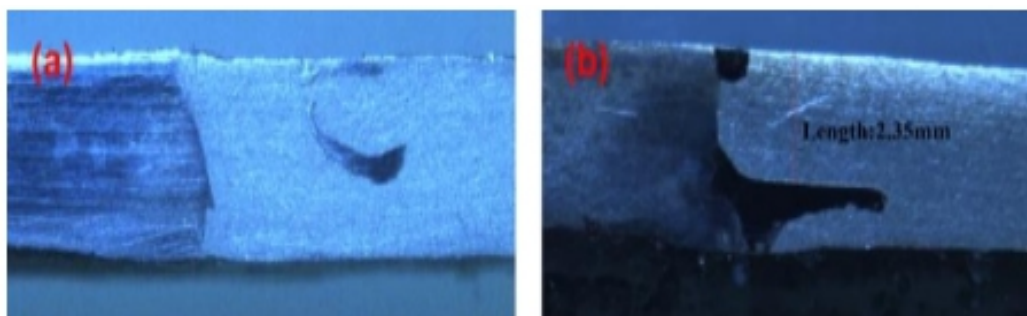


**Fig. 6 Macrograph of FSW joint (a) By normal FSW, (b) By Induction Heating Assisted FSW**

Scanning electron microscope images of normal Al-Steel FSW joint (A1-A3) and IHAFSW joint (B1-B3) are shown in Fig. 7. On analyzing interface micrographs obtained at high magnification SEM, a continuous bonding surface was apparent without the presence of an intermetallic layer. Further high magnification showed intermittent microcracks along the joint line, which is an intrinsic attribute of a dissimilar weld joint. Even though microcracks are present in both the cases, the joint performed using IHAFSW has a lesser number of crack sites as compared to normal FSW joint interface. This indicated a relatively better bonding in IHAFSW.

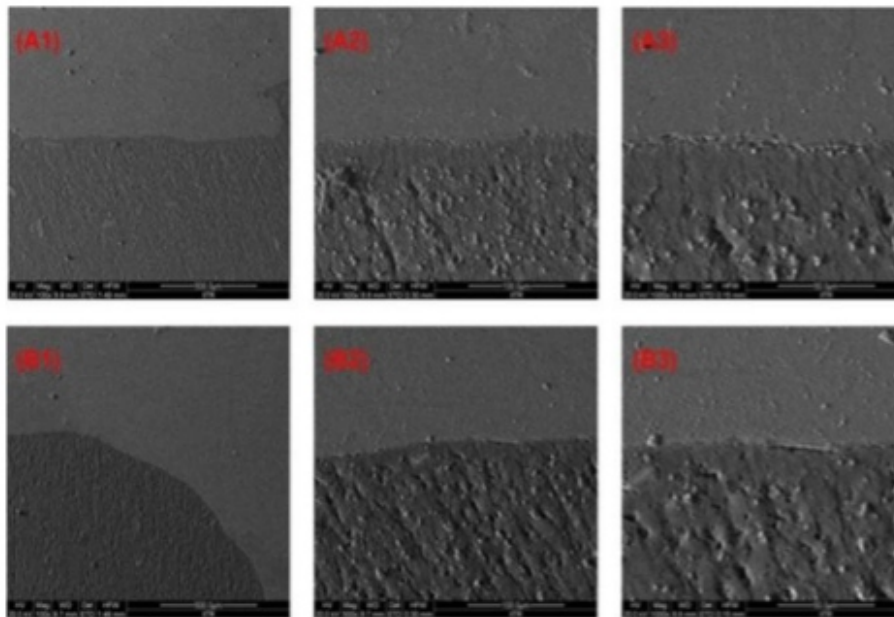


**Fig. 7 (A) SEM micrograph of the interface of normal FSW joint at different magnification, (B) SEM micrograph of the interface of IHAFSW joint at different magnification**

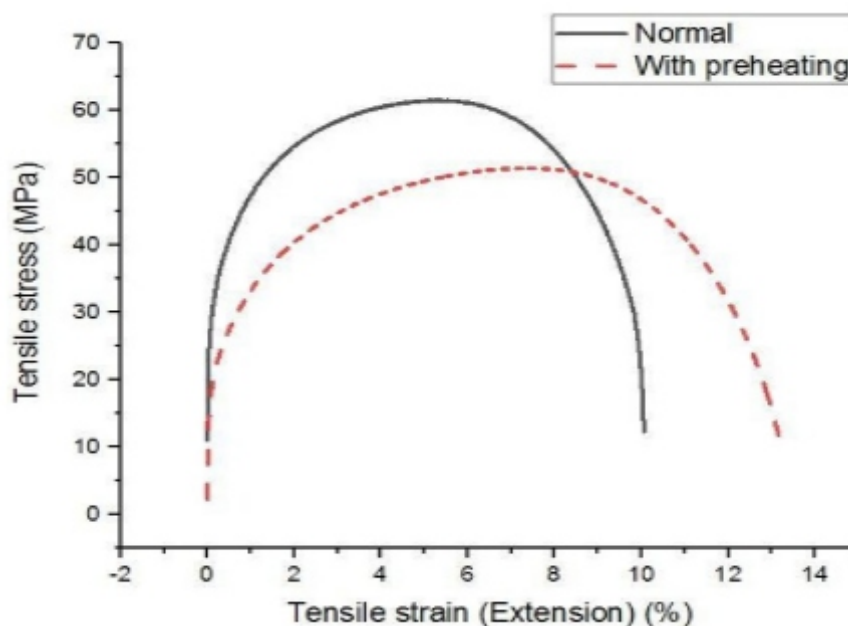


**Fig. 8 Tensile test graph of normal FSW joint and Induction preheated FSW joint**

---

The results of the tensile test of normal FSW joint and induction heat-assisted FSW joint are plotted in Fig. 8. It was perceived from the tensile test that the elongation of IHAFSW joint was superior to the normal FSW joint. Tensile strain in IHAFSW joint was found to be around 13.5%. It showed an improvement of 35% over normal FSW joint extension. Although the strength of IHAFSW joint was somewhat inferior to the normal FSW joint which indicated softening of the joint.

#### IV. CONCLUSION

On the basis of experiments performed for joining of Al-steel dissimilar combination, following conclusive points are drawn:

- Steel has higher flow stress and hardness than the aluminum, therefore for achieving better stirring action during Friction stir welding, flow stress of steel is to be brought in comparison to aluminum by using some external heating source.
- Induction heating process prior to friction stir welding is a suitable alternative for performing selective preheating because of its capability to heat only magnetic (steel) plate.
- Around 35% improvement in the ductility of FSW joint was obtained on the application of selective induction preheating of steel plate.

#### REFERENCES

- [1] Y. Kusuda, "Honda develops robotized FSW technology to weld steel and aluminum and applied it to a mass-production vehicle," *Ind. Rob.*, vol. 40, no. 3, pp. 208–212, 2013.
- [2] "Engineering ToolBox, (2005). Metals - Melting Temperatures. [online] Available at: [https://www.engineeringtoolbox.com/melting-temperature-metals-d\\_860.html](https://www.engineeringtoolbox.com/melting-temperature-metals-d_860.html) [Accessed 25/04/2019].," 2018. .
- [3] H. S. Bang, H. S. Bang, G. H. Jeon, I. H. Oh, and C. S. Ro, "Gas tungsten arc welding assisted hybrid friction stir welding of dissimilar materials Al6061-T6 aluminum alloy and STS304 stainless steel," *Mater. Des.*, vol. 37, pp. 48–55, 2012.
- [4] J. Luo, W. Chen, and G. Fu, "Hybrid-heat effects on electrical-current aided friction stir welding of steel, and Al and Mg alloys," *J. Mater. Process. Technol.*, vol. 214, no. 12, pp. 3002–3012, 2014.
- [5] X. Liu, S. Lan, and J. Ni, "Electrically assisted friction stir welding for joining Al 6061 to TRIP 780 steel," *J. Mater. Process. Technol.*, vol. 219, pp. 112–123, 2015.
- [6] "Engineering ToolBox, (2008). Temperature and Strength of Metals. [online] Available at: [https://www.engineeringtoolbox.com/metal-temperature-strength-d\\_1353.html](https://www.engineeringtoolbox.com/metal-temperature-strength-d_1353.html) [Accessed 15/04/2019]."
- [7] D. MANNAN, "Pressure system design," in *Lees' Loss Prevention in the Process Industries*, Elsevier, 2007, pp. 1–104.

---

---

# Geometro Thermodynamics of the Boltzmann-GIBBS and Pareto Distributions

**Maria N. Quevedo**

<sup>1</sup>Departamentode Matemáticas, Universidad Militar Nueva Granada, Cra. 11 No. 101-80, Bogotá D.E., Colombia E-mail: maria.quevedo@unimilitar.edu.co

## **ABSTRACT**

*The formalism of geometro thermodynamics is used to derive Riemannian metrics for the equilibrium spaces of thermodynamic systems described by the Boltzmann-Gibbs and Pareto distributions, which are widely used in econophysics. We thus show that the corresponding equilibrium spaces are, in fact, Riemannian differential manifolds for which we can calculate the respective curvature. In the case of the Boltzmann-Gibbs distribution, we show that the curvature vanishes so that the manifold is globally flat. In the case of the Pareto distribution, the curvature is non-zero and singularities are present for a wide range of values of the Pareto parameter. We thus show that it is possible to characterize these distributions by using the geometric properties of the corresponding equilibrium manifolds.*

**Keywords - Boltzmann-Gibbs Distribution, Pareto distribution, Econophysics, Geometrothermo dynamics.**

## **I. INTRODUCTION**

Differential geometry is a very important tool of modern science, specially of mathematical physics, with many applications in physics, chemistry and engineering. Consider, for instance, thermodynamics, the branch of physics that studies all the systems in the Universe, where the laws of thermodynamics are valid. This includes microscopic configurations such as quantum gases, condensates, etc., classical laboratory gases and liquids and even the largest known system which is the Universe itself. To study thermodynamic systems from a geometric point of view, one introduces the concept of equilibrium space, each point of which represents an equilibrium state of the system.

In turn, to investigate the equilibrium space there are essentially two methods. The first one is named thermodynamic geometry and consists in introducing Riemannian metrics into the equilibrium space. In general, the components of the Riemannian metrics are taken as the components of a Hessian matrix, i.e., the second derivatives of a function, which is usually assumed to coincide with a thermodynamic potential, for instance, the entropy or the internal energy. Hessian metrics have been applied to investigate many physical systems and very interesting results have been obtained (see, for instance, [1]-[3] for comprehensive reviews).

The second approach is called geometrothermo- dynamics (GTD) and is based upon the use of Legendre invariance, i.e., the property that classical thermodynamics does not depend on the choice of

---

thermodynamic potential [4]. To represent Legendre invariance as an invariance with respect to coordinate transformations, it is necessary to introduce an auxiliary space which is called phase space. A metric, which is Legendre invariant in the phase space, contains the symmetry properties of classical thermodynamics with respect to changes of thermodynamic potential. We equip in this way the equilibrium space with Legendre invariant metrics. It turns out that the components of the metric can essentially be calculated once the fundamental equation [5] of the corresponding thermodynamic system is given.

In turn, the fundamental equation can be derived by using the approach of statistical thermodynamics, if the distribution function is known [6]. In this work, we are interested in the Boltzmann-Gibbs and Pareto distributions, which have been used in the framework of econophysics to describe the distribution of certain economic variables along the population of a society. In fact, it is currently well established that the wealth distribution in many societies presents essentially two phases [7]. This means that the society can be differentiated in two disjoint populations with two different probability distributions. Various analysis of real economic data from several countries have shown that one phase possesses a Boltzmann-Gibbs (exponential) probability distribution that involves about 95% of individuals, mostly those with medium and low wealth, whereas the second phase, consisting of about 5% of individuals with highest wealth, shows a Pareto (power law) probability distribution. Similar results are found for the distribution of money and income. It follows that it is important to understand the properties of the Boltzmann-Gibbs and Pareto distributions to describe the behavior of economic systems. This is one of the main goals of the present study.

In this work, we are interested in investigating the Boltzmann-Gibbs and Pareto distributions from the point of view of GTD. To this end, we first present in Section II a review of the GTD formalism. Then, in Section III, we describe the method we use to derive the fundamental equation corresponding to a particular function distribution. In Section IV, we calculate the metrics which describe the geometric properties of Boltzmann-Gibbs and Pareto equilibrium spaces, respectively.

## **II. GEOMETROTHERMODYNAMICS**

GTD is a theory that has been formulated recently in [4] to introduce, in a consistent manner, Legendre invariance in the geometric description of the space of thermodynamic equilibrium states. This theory has been applied to different thermodynamic systems such as black holes, ideal and realistic gases, chemical reactions and even the entire Universe. In all the cases analyzed so far, GTD has delivered consistent results and allows us to describe geometrically thermodynamic interaction and phase transitions by means of Legendre invariant metrics.

The main ingredient of GTD is a  $(2n+1)$ -dimensional manifold  $T$  with coordinates  $Z^A = (\Phi, E^a, I^a)$ , where  $\Phi$  is an arbitrary thermodynamic potential,  $E^a$ ,  $a = 1, 2, 3, \dots$ , are the extensive variables, and  $I^a$  the intensive variables that are used to describe thermodynamic systems. It is also possible to introduce in a canonical manner the fundamental one-form

$$\Theta = d\Phi - \delta_{ab} I^a dE^b,$$

$$\delta_{ab} = \text{diag} +1, \dots, +1, \dots$$

which satisfies the condition  $\Theta \wedge d\Theta \neq 0$ , where  $n$  is the number of thermodynamic degrees of freedom of the system, and is invariant with respect to total Legendre transformations

$$(\Phi, E^a, I^a) \rightarrow \Phi, E^a, I^a$$

with

$$\Phi = \Phi - \delta_{ab} E^a I^b, \quad E^a = -I^a, \quad I^a = E^a.$$

Partial Legendre transformations can be represented as particular cases. Moreover, we assume that on  $T$  there exists a metric  $G$ , which is also invariant with respect to Legendre transformations. The triad  $(T, \Theta, G)$  defines a Riemannian contact manifold which is called the thermodynamic phase space (phase manifold). The space of thermodynamic equilibrium states (equilibrium manifold) is defined as an  $n$ -dimensional Riemannian submanifold,  $E \subset T$ , induced by a smooth map

$$\varphi: E \rightarrow T, \text{ i.e. } \varphi: (E^a) \mapsto (\Phi(E^a), E^a, I^a(E^a)), \text{ such}$$

that

$$\varphi^* \Theta = \varphi^* d\Phi - \delta_{ab} I^a dE^b = 0$$

holds, where  $\varphi^*$  is the pullback of  $\varphi$ . The manifold  $E$  is naturally equipped with the Riemannian metric  $g = \varphi^* G$ .

The purpose of GTD is to demonstrate that the geometric properties of  $E$  are related to the thermodynamic properties of a system with fundamental thermodynamic equation  $\Phi = \Phi(E^a)$ .

It turns out that there are three classes of Legendre invariant metrics, namely,

$$G^{I\text{I}} = (d\Phi - I_a dE^a)^2 + (\xi_{ab} E^a I^b) (\chi_{cd} dE^c dI^d)$$

which are invariant under total Legendre transformations, where  $\xi_{ab}$  and  $\chi_{ab}$  are diagonal constant matrices. For  $\chi_{ab} = \delta_{ab} = \text{diag}(1, \dots, 1)$  or  $\chi_{ab} = \eta_{ab} = \text{diag}(-1, 1, \dots, 1)$ , the resulting metric  $G^I$  or  $G^{\text{II}}$  can be used to investigate systems with at least one first-order or second-order phase transition, respectively. The third class

$$G^{\text{III}} = (d\Phi - I_a dE^a)^2 + (E_a I_a)^{2k+1} dE^a dI^a, k \in \mathbb{Z}$$

is invariant with respect to partial Legendre transformations and is used to describe ordinary systems.

The calculation of the metrics for the equilibrium space is straightforward and yields

$$g^{I\text{II}} = \beta_{\Phi} \Phi \xi^c \Phi \quad dE^a dE^b = \beta \quad \Phi \xi^c \frac{\partial^2 \Phi}{\partial E^b \partial E^c} dE^a dE^b$$

where  $\beta_{\Phi}$  is a constant and  $\xi_c = \delta_c = \text{diag}(1, \dots, 1)$  for  $g^I$  and  $\xi_c = \eta_c = \text{diag}(-1, 1, \dots, 1)$  for  $g^{II}$ . These metrics are invariant with respect to total transformations. Furthermore, from the metric  $G^{III}$ , we obtain

$$g^{III} = (E \Phi_a)^{2k+1} \delta^{ab} \Phi_{bc} dE^a dE^c$$

where

$$\Phi_a = \frac{\partial \Phi}{\partial E^a}, \quad \Phi_{bc} = \frac{\partial^2 \Phi}{\partial E^b \partial E^c}$$

We can see that all metrics  $g$  can be calculated explicitly once the fundamental equation  $\Phi(E^a)$  is known.

### III. BOLTZMANN-GIBBS AND PARETO FUNDAMENTAL EQUATIONS

In [6], it was proposed to use the approach of statistical thermodynamics to derive fundamental equations of thermodynamic systems. The idea is as follows. Suppose that the system is composed of  $N$  elements and each element possesses a part  $m$  of a conserved quantity  $M$ . If the system is at equilibrium, the probability distribution (density function)  $\rho(m)$  is essentially given as  $\rho(m) = e^{-m/T}$ , where  $T$  is the average amount  $M/N$ . The amount  $m$  can depend on several additional parameters  $\lambda_1, \lambda_2, \dots, \lambda_3$ , which are usually called microeconomic parameters. Since the density function can be normalized to 1, we obtain [8]

$$\rho(\lambda) = \frac{e^{-m(\lambda)T}}{Q(T, \mathbf{x})}, \quad Q(T, \mathbf{x}) = \int e^{-m(\lambda)T} d(\lambda),$$

where  $Q(T, \mathbf{x})$  is the partition function and  $\lambda$  represents the set of all microeconomic parameters. Here we introduced the notation  $\mathbf{x} = x_1, x_2, \dots, x_n$  to denote the set of macroeconomic parameters that can appear after the integration over the entire domain of definition of the microscopic parameters  $\lambda$ .

Following the standard procedure of statistical thermodynamics [8], we introduce the concept of mean value  $g$  for any function  $g = g(\lambda)$  as

$$g = \int g \rho d\lambda = \frac{1}{Q(T, \mathbf{x})} \int g e^{-m(\lambda)T} d\lambda$$

In statistical thermodynamics, these are the main concepts used to investigate systems which depend on the average  $T$  and the macroscopic variables  $\mathbf{x}$ . Consider, for instance, the mean value  $m = \int m \rho d\lambda$  and compute the total differential  $dm$ ,

$$dm = m d\rho + \rho dm = m d\rho + \rho dm$$

By using the equation  $m = -T(\ln \rho + \ln Q)$ , the above expression can be written as

$$dm = T dS - \sum_{i=1}^n y_i dx_i$$

where the entropy  $S$  and the intensive macroscopic variables are defined as

$$S = -\ln \rho = -\ln \rho \, d\lambda$$

and

$$y_i = -\frac{\partial m}{\partial x_i} = -\frac{\partial m}{\partial x_i} \rho \, d\lambda.$$

This is the first law of thermodynamics. To calculate explicitly the entropy  $S = -\ln \rho \, d\lambda$ , we use the equation  $-\ln \rho = \ln Q + m/T$  and obtain  $f = m - TS = -T \ln Q(T, x)$ , so that

$$S = -\frac{\partial f}{\partial T} \cdot y_i = -\frac{\partial f}{\partial x_i}$$

This means that the entire information about the thermodynamic properties of the system is contained in the function  $m(\lambda)$  which, in turn, is completely determined by the partition function  $Q(T, x)$ . We see that to find all the relevant thermodynamic variables, it is necessary to specify only the function  $m$ .

To generate the Boltzmann-Gibbs distribution, we consider the linear function  $m = c_1 \lambda_1$  which leads to the partition function

$$Q(T, \Lambda) = \frac{T\Lambda}{c_1 \Lambda_1} e^{-\frac{c_1}{T} \lambda_1} \Big|_{\lambda_1^{\min}}^{\lambda_1^{\max}}$$

Then, the corresponding thermodynamic variables are

$$S = 1 + \ln \frac{\langle m \rangle}{C_1} + \ln \Lambda$$

where we have considered  $\lambda_1$  in the interval  $[0, \infty)$  for simplicity. Here  $\Lambda$  is an additional thermodynamic variable which comes from the integration along the microscopic parameters. The above expression represents the fundamental equation of the Boltzmann-Gibbs distribution, which depends on the extensive variables  $\langle m \rangle$  and  $\Lambda$ .

An important quantity that reflects the phase transition properties of the system is the capacity, which is defined as

$$C = T \frac{\partial S}{\partial T}$$

If we calculate this quantity for the Boltzmann-Gibbs entropy function, we obtain  $C = 1$ . This means that no phase transitions can occur in a system described by this distribution function. Consider now a system determined by the multiplicative function  $m = c_1 \ln \lambda_1$ . Then, the partition function is given by

$$\begin{aligned} Q(T, \Lambda) &= \int e^{-c_1 \lambda_1 / T} d\lambda_1 = \frac{\Lambda}{\Lambda_1} e^{-c_1 \lambda_1 / T} \\ &= \frac{T\Lambda}{c_1 \Lambda_1} \end{aligned}$$

where we have used  $\lambda_1 \in [x, \infty)$ , with  $x = \lambda^{\min}$ . This expression is completely equivalent to the Pareto distribution function. As mentioned above, our method allows us to find the corresponding thermodynamic potential in terms of the macroscopic parameters. In particular, the entropy is given by

$$S = \frac{c_1}{-T} e^{-T} + \ln \frac{xT}{c_1 - T} + \ln \Lambda,$$

where the average  $T$  is, in turn, a function of  $\langle m \rangle$  and  $x$ , i.e.,

$$T = c_1 \frac{\langle m \rangle - c_1 \ln x}{\langle m \rangle + c_1 - c_1 \ln x}.$$

Then, the entropy function  $S = S(\langle m \rangle, x, \Lambda)$  represents the fundamental equation for the Pare to distribution. The main variables in this case are  $\langle m \rangle$  and  $x$  and we will focus on them for our further analysis. In this case, the capacity  $C$  can be calculated from the entropy function and we obtain

$$C = \frac{c_1^2}{c_1 - T},$$

an expression which diverges for  $T = c_1$ , indicating the presence of a second-order phase transition.

#### IV. METRICS OF THE EQUILIBRIUM SPACE

To describe a system in GTD, it is necessary to determine the metric to be used and this, in turn, depends of the kind of phase transitions that are present in the system. Consider a Boltzmann-Gibbs system for which we found in the last section that the capacity is constant ( $C = 1$ ). Then, such a system has no phase transitions and, therefore, corresponds in GTD to a system invariant with respect to partial and total Legendre transformations with metric  $g^{\text{III}}$ . If we now identify the variables  $\Phi = S$ ,  $E^1 = \langle m \rangle$ , and  $E^2 = \Lambda$ , and use the fundamental equation for the Boltzmann-Gibbs distribution, we obtain

$$g^{\text{III}} = - \frac{d \langle m \rangle^2}{\langle m \rangle^2} + \frac{d \Lambda^2}{\Lambda^2}$$

To calculate the curvature tensor and the curvature scalar, we use the standard formulas of Riemannian geometry. For the above metric, one can show that the curvature tensor is zero, i.e., the corresponding equilibrium space is flat. In GTD, this is interpreted as corresponding to a system without intrinsic interaction. Consider now the Pareto fundamental equation  $S = S(\langle m \rangle, x)$ . As mentioned above, in this case the capacity indicates the presence of second order phase transitions. We therefore use the metric  $g^{\text{II}}$  for its description. In the general formula for  $g^{\text{II}}$  given above, we make the identification  $\Phi = S$ ,  $E^1 = \langle m \rangle$  and  $E^2 = x$ . The calculation of the metric components yields

$$g^{\text{II}} = \frac{S(\langle m \rangle, x)}{c_1 \ln x - \langle m \rangle^2} d \langle m \rangle^2 - c_1 c_1 \ln x + c_1 - \langle m \rangle \frac{dx^2}{x^2},$$

---

for which we calculate the curvature scalar

$$R = \frac{N(\langle m \rangle, x)}{c_1 \ln x + c_1 - \langle m \rangle^2}$$

where the function  $N(\langle m \rangle, x)$  is different from zero, in general. We see that curvature singularities occur for all the values of  $\langle m \rangle$  and  $x$ , which satisfy the condition

$$c_1 \ln x + c_1 - \langle m \rangle^2 = 0.$$

We conclude that systems described by the Pareto distribution function show a very rich phase transition structure.

## V. CONCLUSION

In this work, we used the formalism of GTD to derive the Legendre invariant metrics that describe the equilibrium space of systems which satisfy the Boltzmann-Gibbs and the Pareto probability distribution functions. First, by using the methods of statistical thermodynamics, from the distribution function we derive the corresponding fundamental equation, i.e., a function that relates the entropy with the remaining extensive variables of the system. From the fundamental equation one can calculate the corresponding metric for the equilibrium space by using GTD. We found that the Boltzmann-Gibbs distribution leads to flat equilibrium space, indicating the lack of intrinsic interaction between the elements of the system. On the contrary, the Pareto distribution is described by a metric with non-vanishing curvature and a very rich phase transition structure.

As mentioned above, the Boltzmann-Gibbs and Pareto distributions play an important role in econophysics. In this context, it would be interesting to analyze the consequences of the completely different geometric properties of these distributions.

## ACKNOWLEDGEMENTS

This work was carried out within the scope of the project CIAS 2546 supported by the Vicerrectoría de Investigaciones de la Universidad Militar Nueva Granada-Vigencia 2018.

## REFERENCE

- [1] S. Amari, *Differential-Geometrical Methods in Statistics* (Springer-Verlag, Berlin, 1985).
- [2] F. Weinhold, *Classical and Geometrical Theory of Chemical and Phase Thermodynamics* (Wiley, Hoboken, New Jersey, 2009).
- [3] G. Ruppeiner, *Springer Proc. Phys.* 153, 179 (2014). [4] H. Quevedo, *J. Math. Phys.* 48, 013506 (2007).
- [5] H.B. Callen, *Thermodynamics and an Introduction to Thermostatistics* (John Wiley & Sons, Inc., NY, 1985).
- [6] H. Quevedo and M. N. Quevedo, *Electr. J. Theor. Phys.* 2011, 1-16 (2011).
- [7] A. Dragulescu and V. M. Yakovenko, *Statistical mechanics of money*, *Eur. Phys. J. B* 17, 723 (2000).
- [8] K. Huang, *Statistical mechanics* (John Wiley & Sons, New York, 1987).

# Instructions for Authors

## Essentials for Publishing in this Journal

- 1 Submitted articles should not have been previously published or be currently under consideration for publication elsewhere.
- 2 Conference papers may only be submitted if the paper has been completely re-written (taken to mean more than 50%) and the author has cleared any necessary permission with the copyright owner if it has been previously copyrighted.
- 3 All our articles are refereed through a double-blind process.
- 4 All authors must declare they have read and agreed to the content of the submitted article and must sign a declaration correspond to the originality of the article.

## Submission Process

All articles for this journal must be submitted using our online submissions system. <http://enrichedpub.com/> . Please use the Submit Your Article link in the Author Service area.

---

## Manuscript Guidelines

The instructions to authors about the article preparation for publication in the Manuscripts are submitted online, through the e-Ur (Electronic editing) system, developed by **Enriched Publications Pvt. Ltd.** The article should contain the abstract with keywords, introduction, body, conclusion, references and the summary in English language (without heading and subheading enumeration). The article length should not exceed 16 pages of A4 paper format.

### Title

The title should be informative. It is in both Journal's and author's best interest to use terms suitable. For indexing and word search. If there are no such terms in the title, the author is strongly advised to add a subtitle. The title should be given in English as well. The titles precede the abstract and the summary in an appropriate language.

### Letterhead Title

The letterhead title is given at a top of each page for easier identification of article copies in an Electronic form in particular. It contains the author's surname and first name initial .article title, journal title and collation (year, volume, and issue, first and last page). The journal and article titles can be given in a shortened form.

### Author's Name

Full name(s) of author(s) should be used. It is advisable to give the middle initial. Names are given in their original form.

### Contact Details

The postal address or the e-mail address of the author (usually of the first one if there are more Authors) is given in the footnote at the bottom of the first page.

### Type of Articles

Classification of articles is a duty of the editorial staff and is of special importance. Referees and the members of the editorial staff, or section editors, can propose a category, but the editor-in-chief has the sole responsibility for their classification. Journal articles are classified as follows:

#### Scientific articles:

1. Original scientific paper (giving the previously unpublished results of the author's own research based on management methods).
2. Survey paper (giving an original, detailed and critical view of a research problem or an area to which the author has made a contribution visible through his self-citation);
3. Short or preliminary communication (original management paper of full format but of a smaller extent or of a preliminary character);
4. Scientific critique or forum (discussion on a particular scientific topic, based exclusively on management argumentation) and commentaries. Exceptionally, in particular areas, a scientific paper in the Journal can be in a form of a monograph or a critical edition of scientific data (historical, archival, lexicographic, bibliographic, data survey, etc.) which were unknown or hardly accessible for scientific research.

**Professional articles:**

1. Professional paper (contribution offering experience useful for improvement of professional practice but not necessarily based on scientific methods);
2. Informative contribution (editorial, commentary, etc.);
3. Review (of a book, software, case study, scientific event, etc.)

**Language**

The article should be in English. The grammar and style of the article should be of good quality. The systematized text should be without abbreviations (except standard ones). All measurements must be in SI units. The sequence of formulae is denoted in Arabic numerals in parentheses on the right-hand side.

**Abstract and Summary**

An abstract is a concise informative presentation of the article content for fast and accurate Evaluation of its relevance. It is both in the Editorial Office's and the author's best interest for an abstract to contain terms often used for indexing and article search. The abstract describes the purpose of the study and the methods, outlines the findings and state the conclusions. A 100- to 250-Word abstract should be placed between the title and the keywords with the body text to follow. Besides an abstract are advised to have a summary in English, at the end of the article, after the Reference list. The summary should be structured and long up to 1/10 of the article length (it is more extensive than the abstract).

**Keywords**

Keywords are terms or phrases showing adequately the article content for indexing and search purposes. They should be allocated heaving in mind widely accepted international sources (index, dictionary or thesaurus), such as the Web of Science keyword list for science in general. The higher their usage frequency is the better. Up to 10 keywords immediately follow the abstract and the summary, in respective languages.

**Acknowledgements**

The name and the number of the project or programmed within which the article was realized is given in a separate note at the bottom of the first page together with the name of the institution which financially supported the project or programmed.

**Tables and Illustrations**

All the captions should be in the original language as well as in English, together with the texts in illustrations if possible. Tables are typed in the same style as the text and are denoted by numerals at the top. Photographs and drawings, placed appropriately in the text, should be clear, precise and suitable for reproduction. Drawings should be created in Word or Corel.

**Citation in the Text**

Citation in the text must be uniform. When citing references in the text, use the reference number set in square brackets from the Reference list at the end of the article.

**Footnotes**

Footnotes are given at the bottom of the page with the text they refer to. They can contain less relevant details, additional explanations or used sources (e.g. scientific material, manuals). They cannot replace the cited literature.

The article should be accompanied with a cover letter with the information about the author(s): surname, middle initial, first name, and citizen personal number, rank, title, e-mail address, and affiliation address, home address including municipality, phone number in the office and at home (or a mobile phone number). The cover letter should state the type of the article and tell which illustrations are original and which are not.

**Address of the Editorial Office:**

**Enriched Publications Pvt. Ltd.**  
S-9, IInd FLOOR, MLU POCKET,  
MANISH ABHINAV PLAZA-II, ABOVE FEDERAL BANK,  
PLOT NO-5, SECTOR -5, DWARKA, NEW DELHI, INDIA-110075,  
PHONE: - + (91)-(11)-45525005